Multi-physics modeling of the ignition of polymer matrix composites (PMCs) exposed to fire

J. Langot[a,*], T. Pelzmann[a], P. Chávez-Gómez[a], C.S. Boanta[a], J. Karsten[b], B. Fiedler[b], M. Lévesque[a], E. Robert[a]

[a] *Polytechnique Montréal, 2500 chemin de Polytechnique, H3T 1J4 Montréal (Canada)*
[b] *Hamburg University of Technology, Institute of Polymers and Composites, 21073 Hamburg (Germany)*

Abstract

Advanced polymer matrix composites (PMCs) are widely used in modern aircraft and as such have to withstand fire to comply with safety regulations. The thermal degradation of these lightweight materials is a complex process involving chemical reactions in the solid and gas phases, potentially leading to flaming combustion. Here, we numerically investigate the heat feedback from the ignition of outgassing at the surface of a structural polymer matrix composite exposed to a pilot flame. Our model couples the thermal, physical and chemical processes in the solid phase to compute the composite degradation, as well as the production and movements of pyrolysates. A counterflow diffusion flame is used to model the ignition of the combustible effluent close to the sample surface, where the hot jet of the pilot flame impinges. The predictive capabilities of the method are demonstrated considering a carbon/epoxy composite subjected to a small-scale fire test. As input data for our model, material properties have been measured for virgin and partially burned samples via Differential Scanning Calorimetry, Xenon Flash Analysis and Thermogravimetric Analysis. The model is able to predict the backface temperature and time-to-ignition of the composite sample exposed to a flame with a good deegre of accuracy.

Keywords: Pyrolysate combustion, Pyrolysis model, Chemical kinetics model, GRI-Mech

---

*Corresponding author:
Email address: `jean.langot@polymtl.ca` (J. Langot)

3.0, Fire test, Heat feedback, time-to-ignition, carbon/epoxy, polymer matrix composites (PMCs)

---

1. Introduction

Polymer matrix composites (PMC) are extensively used in the aerospace industry due to their light weight and versatility [1]. However, owing to their inherent flammability, their usage is mostly limited to applications where temperatures do not reach their glass transition T_g nor decomposition temperatures [2]. To decrease aircraft weight, there is an incentive to use these materials in location where they must act as firewalls, such as in and around powerplants. In such cases, their fire resistance is assessed through standardized certification tests requiring the material to maintain its fire-blocking functions when exposed to a 1366 K (2000 °F) pilot flame for 15 minutes [3]. To increase the understanding of failure modes and improve the design process of PMC-based aircraft powerplant firewalls, this paper presents a multi-physics model for the thermo-chemical decomposition processes associated with a carbon/epoxy composite subjected to conditions representative of certification tests [3].
When exposed to fire, a PMC undergoes several closely-coupled thermal, chemical and physical processes [4, 5]. As the matrix exceeds its T_g (for amorphous polymers) and the decomposition temperature is reached, it first degrades through pyrolysis, locally decreasing the material density and affecting its thermo-physical properties. The formation of a low-density porous char layer on the surface may protect the remaining matrix from further heat transfer, thus slowing its degradation. Gaseous pyrolysis products (henceforth referred to as *pyrolysates*) migrate from the inside of the material toward the hot face as a consequence of pressure gradients and higher permeability in this direction. The combustible effluent exiting the sample meets the hot exhaust jet produced by the pilot flame close to the surface. The pilot burner is operated lean to achieve the desired temperature. Consequently, the gaseous exhaust effluent contains non-negligible amounts of oxygen. Moreover, as the pilot flame itself approaches the surface, other oxidative species besides O_2 as well as radicals are

available to mix with and ignite the pyrolysate escaping the surface. This reactive mixture ignites as the lower flammability limit is reached and gives rise to a diffusion flame which in turn provides a heat feedback further promoting the material degradation. The ignition of the composite is defined as the onset of self-sustained combustion, potentially leading to the appearance of large flames that may contribute to spread fire. Consequently, the time-to-ignition is an important parameter in fire safety science [6]. The temperature of the flame produced by this additional heat source depends on the pyrolysate composition and fire test conditions. The thermal feedback loop is also a crucial factor in the fire resistance of combustible solids and its accurate modeling is paramount to achieve quantitative predictions. Finally, the char and, subsequently, carbon fibers are oxidized, increasing again the material porosity and providing an additional heat source due to the exothermic nature of these oxidation reactions. So-called *pyrolysis models* aim at modeling the interactions between these processes [7–10].

The thermal degradation of PMCs has been studied considering materials exposed to both non-reactive and reactive heat sources [11–17]. Non-reactive heat sources are often lasers [11, 12] or radiant heaters [13, 14]. The models considering these heat sources usually offer good agreement with experimental data since a non-reactive source is often simpler to model than a reactive one. Indeed, the source heat flux is typically homogeneous and the atmosphere can be controlled to prevent oxidation or pyrolysate ignition, which considerably limits the number and complexity of phenomena that must be modeled. By contrast, the modeling of reactive heat sources, such as pilot flames, is much more challenging [15–17], notably because the interactions between the flame and the pyrolysate strongly affect the composite ignition. The thermal degradation of composites is sensitive to the heat feedback from pyrolysate combustion [18, 19], which depends on the nature of the material exposed to heat [20]. In the context of a fire test, the pyrolysate combustion for a given material is also affected by the composition of the exhaust gases from the pilot flame, which in turn depends on burner operation parameters [3, 21]. In previous modeling of a fire test, pyrolysate com-

bustion was often neglected [15, 16] or modeled with empirical parameters [17] that must be inferred experimentally for each set of test conditions and material composition. Fully coupled solid-gas models have also been developed for the piloted ignition of combustible materials [12, 18–20, 22, 23], but they often relied on simplified chemical kinetics, i.e. global one-step reactions, that cannot capture the effect of composition in the exhaust gases of a burner used for certification testing. This simplification has two consequences; first, it can lead to an overestimation of the flame temperature from pyrolysate combustion, as global one-step reactions do not consider the heat absorbed by the endothermic dissociation reactions. Second, the pyrolysate time-to-ignition cannot be modeled with a global one-step reaction. A mixture ignites when the heat generated by chemical reactions exceeds heat losses, favoring the creation of chain carriers leading to thermal runaway. As a consequence, chemical kinetics based on global one-step reaction relies again on empirical parameters to estimate the time-to-ignition [24], usually related to a critical pyrolysate mass flow rate [25] or material surface temperature [26].

Available general purpose complex reaction mechanisms are suitable to model pyrolysate ignition and combustion. For instance, GRI-Mech 3.0 has been developed for natural gas combustion and involves 53 species, including hydrocarbons up to C3, and 325 reactions [27]. These mechanisms can be implemented in two- or three-dimensional Computational Fluid Dynamics (CFD) simulations, but such modeling in practical combustion applications is a very complex task, with most current simulations limited to flames in simple configurations, with no reacting solid phase [28, 29]. Chemical kinetics software such as Cantera [30] however allows for the use of complex reaction mechanisms in simple one-dimensional CFD simulations, and therefore offer a good compromise between detailed chemical kinetics and accurate CFD simulations. A chemical kinetics software has been coupled to a pyrolysis model by Li *et al.* [31] to investigate the surface ablation of charring composites, but to the best of the authors knowledge the work presented here is the first occurrence that this approach is used to model the heat feedback from pyrolysate ignition in the context of a fire test.

This paper presents a multi-physics model for the heat feedback and time-to-ignition from gas phase reactions at the surface of a composite subjected to a one-sided reactive heat flux. This predictive tool is based on a novel coupling architecture between a pyrolysis model and a chemical kinetics model. Numerical predictions are compared against fire test conducted on a carbon/epoxy composite exposed to a methane flame. For this purpose, a novel small-scale fire test has been developed in another work [21] and used in this study to mimic the conditions encountered in large-scale fire certification [3]. The material has also been characterized extensively to obtain its thermal and chemical properties, both in the virgin state and following thermal degradation. A sensitivity analysis has been done to investigate the effect of variations in material properties, solid-phase chemical reactions and gas-phase chemical reactions. The novelty of this study lies in the coupling architecture of a chemical kinetics software with a pyrolysis model, that has never been done in the context of a fire certification test. This approach allows a purely theoretical prediction of the time-to-ignition and heat feedback from the combustion of pyrolysates mixed with a pilot flame exhaust gases.

2. Background

2.1. Modeling

2.1.1. Pyrolysis models

The degradation of composite materials results from the complex interaction of physical, chemical and thermal processes. This degradation can be modeled empirically [32], but the validity of the model obtained is limited to the conditions of the specific fire test for which it was developed and becomes obsolete if these test conditions are changed. An analytical modeling approach is also possible [33], but it relies on many assumptions, typically restricting its range of application to semi-infinite and non-reactive solids [34]. In contrast, comprehensive models based on the conservation of mass, energy and sometimes momentum [7–10, 12] have a wider range of application, and are adaptable to changes in fire test conditions. However, they require a large number of material properties and parameters that must be inferred

from specialized experiments in simple configurations rather than fire tests. As the predictive tool developed in this work is intended to be adaptable to different fire test conditions, a comprehensive approach is adopted.

2.1.2. Chemical kinetics model

The ignition of combustible materials is driven by chemical reactions occurring in both solid and gas phases. Solid phase reactions are often modeled with global simplified reactions [12, 14, 35] as the chemical species involved are mostly unknown. Gas phase reactions can be modeled with more detailed reaction model such as Cantera, as the pyrolysate composition can be measured [12, 36]. Cantera is an open-source suite of tools, developed for problems involving thermodynamics, transport processes and chemical kinetics [30]. It models flames that are stabilized in an axisymmetric stagnation flow, and computes the solution along the stagnation streamline ($r = 0$), using a similarity solution to reduce the three-dimensional governing equations to a single dimension. In particular, the counterflow diffusion flame sub-model (class *CounterflowDiffusionFlame* in Python) is governed by the conservation of mass, radial momentum, energy and species, which reads:

$$\frac{\partial \rho u}{\partial x} + 2\rho V = 0 \tag{1a}$$

$$\rho u \frac{\partial V}{\partial x} + \rho V^2 = -\Lambda + \frac{\partial}{\partial x}\left(\mu \frac{\partial V}{\partial x}\right) \tag{1b}$$

$$\rho c_p u \frac{\partial T}{\partial x} = \frac{\partial}{\partial x}\left(\lambda \frac{\partial T}{\partial x}\right) - \sum_i j_i c_{p,i} \frac{\partial T}{\partial x} - \sum_i h_i M_i \dot{\omega}_i \tag{1c}$$

$$\rho u \frac{\partial Y_i}{\partial x} = -\frac{\partial j_i}{\partial x} + M_i \dot{\omega}_i \tag{1d}$$

where ρ is the density ($\mathrm{kg\,m^{-3}}$), u and v are the axial and radial velocities ($\mathrm{m\,s^{-1}}$), $V = v/r$ the scaled radial velocity, Λ the pressure eigenvalue ($\mathrm{Pa\,m^{-2}}$), μ the dynamic viscosity ($\mathrm{Pa\,s}$),

T the temperature (K), λ the thermal conductivity ($\mathrm{W\,K^{-1}\,m^{-1}}$), Y_i the mass fraction of species i ($-$), $c_{p,i}$ the specific heat capacity of species i ($\mathrm{J\,kg^{-1}\,K^{-1}}$), h_i the enthalpy of species i ($\mathrm{J\,kg^{-1}}$), M_i the molecular weight of species i ($\mathrm{kg\,mol^{-1}}$) and $\dot{\omega}_i$ the molar production rate of species i ($\mathrm{mol\,m^{-3}\,s^{-1}}$). j_i is the diffusive mass flux of species i ($\mathrm{kg\,m^{-2}\,s^{-1}}$) and is computed with a mixture-averaged formulation. The gases are treated as ideal for the calculation of their thermodynamic properties, following a mixture rule, with polynomial fits used to capture their temperature-dependence. These conservation equations model the transport of matter and heat in the reaction zone. Sin *et al.* [37] showed that similarity solutions can successfully predict velocity profile of a two-dimensional stagnation point flow, even at high aspect ratio (when the distance between inlet and solid surface is 5 times the lateral distance of the problem).

Gas combustion is modeled with the GRI-Mech 3.0. The reaction rates are represented with Arrhenius equations and the chemical equilibrium is modeled with a non-stoichiometric solver [38], yielding the temperature and species distribution in the reaction zone.

2.2. Material characterization

2.2.1. Thermo-physical properties

Each species i contained in the composite (gaseous or solid) needs to be described by at least three thermo-physical properties, depending on the complexity of the pyrolysis model: ρ_i, $c_{p,i}$ and λ_i. Ideally, these properties must be measured as a function of temperature in the range of interest from 300K to 1000K. These temperature-dependent properties are rarely provided by the manufacturer or the literature and an extensive characterization work is therefore necessary. Two different approaches are available to obtain them.

First, the apparent properties of the composite can be used in the predictive tool, without distinction of the different phases [36], reducing the number of thermo-physical properties that must be measured. This method allows the direct use of the properties measured without additional calculation or hypotheses, but cannot provide insight on the properties or degradation of each phase.

The second method consists in calculating the properties of each sub-phases independently from experiments performed on the composite [12, 14], increasing the number of thermo-physical properties that must be measured. This forces the use of conventions and hypotheses to derive all the unknown parameters from a limited number of experiments carried out on the entire composite. The global or *effective* composite properties $\bar{\mathbb{P}}$ can then be determined with a rule of mixture weighted by mass or volume (X_i) fraction:

$$\bar{\mathbb{P}} = \sum_{i=1}^{N} X_i \bar{\mathbb{P}}_i \tag{2a}$$

$$\bar{\mathbb{P}} = \sum_{i=1}^{N} Y_i \bar{\mathbb{P}}_i \tag{2b}$$

where N is the total number of species in the control volume. The mixture rule is the simplest approach to model the composite properties, although it does not account for the geometrical aspects or interactions between phases. Other approaches consider the geometry of the composite with various level of precision. For instance, upper- and lower-bounds of the composite thermal conductivity can be estimated with the Voigt and Reuss models. The Maxwell's model [39] provides the thermal conductivity of a random distribution of spheres into a homogeneous porous media. The Clayton model [40] has been specifically developed and validated [41] for plain-weave composites. Nevertheless, the method consisting in calculating the composite properties as a function of each phase properties increases the complexity of the material characterization, but provides a more detailed insight of the phase contribution to the overall material degradation. Therefore, the second method is preferred in this work. Then, the temperature-dependent thermal conductivities and heat capacities can be measured respectively with Laser/Xenon Flash Analysis (LFA/XFA) [42] and Differential Scanning Calorimetry (DSC) [34].

2.2.2. Kinetic analysis

When exposed to heat, a carbon/epoxy composite degrades through matrix pyrolysis and, if a non-inert atmosphere is considered, this is followed by char oxidation and carbon fiber oxidation. Sensitivity analyses have shown that the matrix pyrolysis plays a dominant role in the composite thermal behavior as char and carbon fibers are comparatively much less reactive [43]. For this reason, among others, char and fibers oxidation were most of the time neglected in composite pyrolysis models [17]. However, in the context of firewall certification testing considered here, a pilot flame can produce species with a high oxidative potential, notably combustion radicals, that can play a significant role in carbon oxidation [44]. Therefore, char and carbon fiber oxidation are included in this work. The reaction rate associated with each chemical reaction is usually computed with the Arrhenius law in pyrolysis models [8–10]:

$$\frac{\partial \alpha}{\partial t} = f(\alpha) A \exp\left(-\frac{E}{RT}\right) \tag{3}$$

where $\alpha = \frac{m(t)-m_0}{m_\infty - m_0}$ is the degree of advancement of the reaction, m_0 and m_∞ are respectively the initial and final mass of the sample (kg), A is the pre-exponential factor (s^{-1}), E the activation energy ($\mathrm{J\,mol^{-1}}$), R the perfect gas constant ($\mathrm{J\,mol^{-1}\,K^{-1}}$). $f(\alpha)$ is the reaction model and represents the dependence of the reaction on the degree of advancement. The reaction model is assumed to follow the n-order law $f(\alpha) = (1-\alpha)^n$ in most pyrolysis models [16, 36, 45], where n is the reaction order ($-$). With this assumption, 3 parameters (A, E, n) must be measured for each reaction, plus a parameter q ($\mathrm{J\,kg^{-1}}$) describing the heat released or absorbed by the chemical reaction. These parameters are usually inferred through Thermogravimetric Analysis (TGA) or Differential Scanning Calorimetry (DSC) using the so-called *isoconversional principle*, which states that the reaction rate at a constant extent of conversion is only a function of temperature [46].

The pyrolysate composition must also be known to model the material ignition. Several authors attempted to measure the composition of the outgassing emitted by an epoxy resin with Mass Spectrometry (MS) [12, 47, 48] or Fourier Transform Infrared spectroscopy

(FTIR) [36, 48–50] and most of them reported the emission of water and some combustible gases such as CH_4 or H_2. However, a qualitative measurement is not sufficient to model the pyrolysate ignition and a quantitative composition is required as input parameter in Cantera. To the best of our knowledge, only two authors provided a quantitative composition of the pyrolysates emitted by the decomposition of an epoxy resin, via MS [12] and FTIR [36], respectively. Tranchard *et al.* [36] provided an average composition of 67.5 vol% of H_2O, 21.3 vol% of CO_2, 3.8 vol% of CO and 2 vol% of CH_4 (among others) with FTIR, for a M21 epoxy resin. It is worth noting that FTIR did not allow to detect H_2, although this species has probably a major influence in pyrolysate ignition because of its reactivity. Schartel *et al.* [49] indicated a strong release of H_2O, phenols and other minor species such as ammonia, CO_2 and hydrocarbons. Ahamad *et al.* [48] identified H_2O, hydrocarbons, CO_2, CO and formaldehyde as the main volatile products. Jiang *et al.*[47] identified H_2O, H_2 and C_2H_2 as the main species present in the pyrolysates with mass spectrometry, using soft ionisation with an electron energy of 15 eV to prevent the fragmentation of hydrocarbons. Pyrolysates are therefore mainly composed of low molecular weight hydrocarbons, which supports the choice of GRI-Mech 3.0 to model their ignition, as this mechanism has been specifically developed for C1-C3 hydrocarbons. From the mass spectrum obtained, Biasi [12] quantified the molar fraction of each of the main species based on the maximum relative intensities of the peaks, therefore considering that the sensitivity of the instrument was identical for all species, an assumption that should be verified through extensive calibration [51]. Although very approximate, such pyrolysate composition obtained is the only one found in the literature for epoxy. It is shown in Table 1 and used in this work as a simplified composition, representative of a typical pyrolysate mixture from epoxy resin. This composition might not burn in air at ambient temperature, but Cantera revealed that this mixture is indeed combustible in an atmosphere composed of hot exhaust gases from the pilot flame, at 1366 K, and containing 15% of oxygen as indicated in Table 2. This is expected as H_2O is a powerful oxidizer at high temperature. The influence of inaccuracies in pyrolysate composition on the

Species	H_2O	H_2	C_2H_2
Volume fraction (−)	0.706	0.199	0.095

Table 1: Composition of the pyrolysates emitted by the pyrolysis of a M21 epoxy resin measured with Mass Spectrometry (from [12]).

modeling of material degradation will be discussed later. Pyrolysates are assumed to be a mixture of ideal gases, so that the volume fraction is equal to the molar composition.

3. Small-scale fire test

Figure 1 represents the small-scale test bench used to reproduce the conditions present in large-scale fire-resistance certification tests [21]. The test considered here is intended for structural components that must act as firewalls and is described in the FAA AC 20-135 [52] and in ISO 2685 [3] standards. The flame is required to have an average temperature of approximately 1100 °C (2000 °F) and a heat flux density of 116 ± 10 kW m^{-2} at the sample location. Although a kerosene burner is traditionally used in certification tests, the flame is produced in this work by a more simple methane burner, as the modeling developed here cannot account for phenomena specific to liquid fuel burners such as droplet projection that could create local hot spots on the sample. The parameters that yield the desired flame conditions are calibrated using a water-calorimeter and a Gardon heat gauge. The sample (25 mm wide and 300 mm long) is held from the top and bottom, with no mechanical stress applied. Two ceramic shields are placed along the sample sides to prevent the flame from wrapping around the edges. The backface temperature opposite to the impinging point is measured continuously using a K-type thermocouple with a spring-loaded joint to maintain steady surface contact. The temperature on the front face is probed only for short times to avoid altering the flame dynamics using a S-type thermocouple, with the exposed wire protected by a ceramic coating. Furthermore, the samples are monitored with video cameras during the entire test duration to identify precisely the ignition onset and the flame quenching at the front face. The small-scale test rig was mounted in an approximately 1 cubic meter enclosure, separated into a hot side where the flame impinges on the sample and the cold

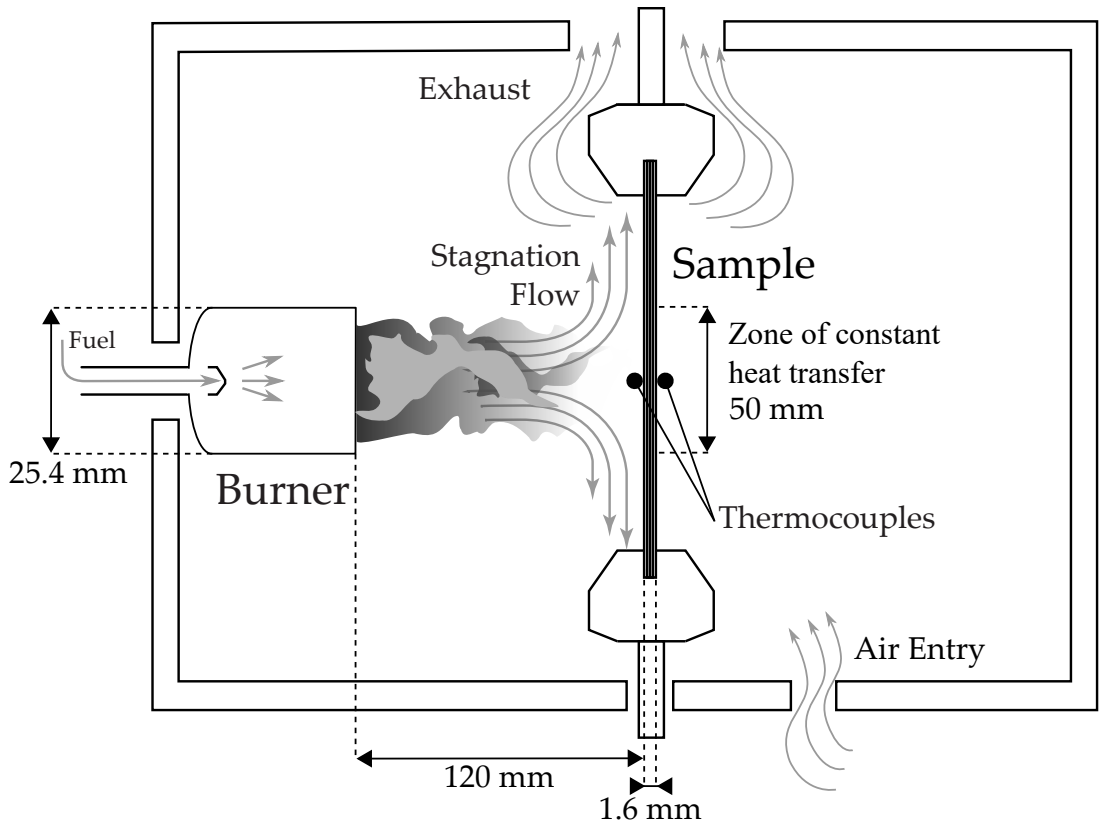

Figure 1: Small-scale test used to reproduce the conditions encountered in real full-scale certification tests.

side where weak outgassing of the sample and natural convection dominated.

4. Modeling

4.1. Coupling architecture

Figure 2 represents the modeling approach implemented here, which consists of three coupled sub-models, as well as the data exchanged. First, a zero-dimensional chemical kinetics model computes the pilot flame chemical equilibrium as a function of the oxidizer and fuel composition (sub-model 1). This model provides the composition of the pilot flame exhaust gases X_b, mass flow rate $\dot{m}_b$ ($\mathrm{kg\,m^{-2}\,s^{-1}}$) and temperature T_b, that are used as input parameters for sub-models 2 and 3. Then, a one-dimensional pyrolysis model computes the thermal decomposition of the composite during fire exposure as a function of the heat flux $\dot{q}_b$ ($\mathrm{W\,m^{-2}}$) received from the pilot flame and pyrolysate ignition at its surface (sub-model 3). This model provides the pyrolysate composition $X_{g,pyr}$, mass flow

rate $\dot{m}_{g,pyr}$ and temperature $T_{g,pyr}$. The one-dimensional computational domain is oriented along the composite sample thickness and co-linear with the pilot flame axis, beginning at the stagnation point of the flame impinging on the hot face and ending on the cold face. The use of a one-dimensional domain in the solid phase is reasonable as the size of the zone of approximately constant heat transfer on the hot face on the order of the pilot flame diameter (50 mm) and the sample width (25 mm) are both much greater than the composite thickness (1.6 mm). Therefore, the lateral dimension of the domain is more than 15 times greater than the axial dimension (along the flame axis), which is greater than the minimum factor of 3 traditionally used to justify the use of one-dimensional domains. In the literature, one-dimensional pyrolysis models have been used successfully to predict the degradation of composites in similar geometrical configurations, exposed to pilot flame [15] or radiant heat flux [14, 53]. Finally, when the pyrolysates flow out of the solid phase and encounter the pilot flame exhaust gases, they form a combustible mixture that can potentially ignite as an axisymmetric non-premixed counterflow flame. A one-dimensional counterflow diffusion flame model is therefore used to identify ignition conditions and provides the flame temperature T_{fl}, which is then used to update the heat flux received by the material $\dot{q}_b$ (sub-model 2). The computational domain for this sub-model begins at the burner exit and ends on the material surface. It is worth noting that similarity solutions reducing a three-dimensional problem to a single dimension have already been used successfully to predict the velocity profile of a two-dimensional stagnation point flow in a similar configuration [37]. This counterflow diffusion flame model limits the use of empirical formulations to model pyrolysate combustion and is intended to make the approach applicable beyond the particular scenario investigated here.

Pyrolysate ignition and heat feedback are modeled as a function of time. The total duration of the fire test is therefore divided into time steps, during which all sub-models exchange data. The pilot flame rapidly reaches steady state and this equilibrium is assumed to be independent from processes in the solid sample or in the thin layer close to the surface where

pyrolysates burn. This hypothesis is reasonable as chemical equilibrium is typically reached in the order of magnitude of 10^{-6} s for methane combustion, which is much faster than the time required to attain the sample surface (in the order of magnitude of 10^{-2} s) or the duration of a time step (not less than 10^{-3} s). The pilot flame sub-model is therefore called only once at the first time step and is not updated thereafter. The chemical processes in the gas phase in the vicinity of the sample surface are assumed to occur very fast relative to the processes in the solid phase, such that the pyrolysate ignition model is computed in steady state, whereas the pyrolysis model in the solid phase is computed in transient state. Therefore, the counterflow diffusion flame and pyrolysis sub-models are called at every time step because, as the material degrades, pyrolysate mass flow rate and temperature evolve over time. The solid and gas phase modeling are combined through a master-slave strong coupling. The solid phase code provides the pyrolysate mass flow rate and temperature on the hot face and calls the counterflow diffusion flame model at each iteration.

4.2. Pilot flame modeling (sub-model 1)

The pilot flame is modeled with the chemical kinetics software Cantera [30], providing the composition and temperature of the exhaust gases at chemical equilibrium. This is achieved using the GRI-MECH 3.0 mechanism (53 species and 325 reactions) with a non-stoechiometric solver, holding pressure and enthalpy fixed (function *equilibrate* in Python). The burner used in this work is a partially premixed methane burner. Both oxidizer (O_2) and fuel are diluted with 55% volume CO_2 to achieve the conditions specified in the certification test procedure in terms of flame temperature and heat flux. The flow rate is 7 Standard Liter Per Minute (SLPM) for both fuel and oxidant mixtures, yielding $\dot{m}_b \approx 0.23\ \mathrm{kg\,m^{-2}\,s^{-1}}$. Air is added to the mixture in Cantera to account for mixing with the atmosphere to reach a flame temperature of 1366 K. The composition of the pilot flame exhaust gases computed by Cantera is provided in Table 2. A study validating such an approach against experimental data for a similar problem has been done by Hu *et al.* [54] and shows good agreement with the Cantera solution.

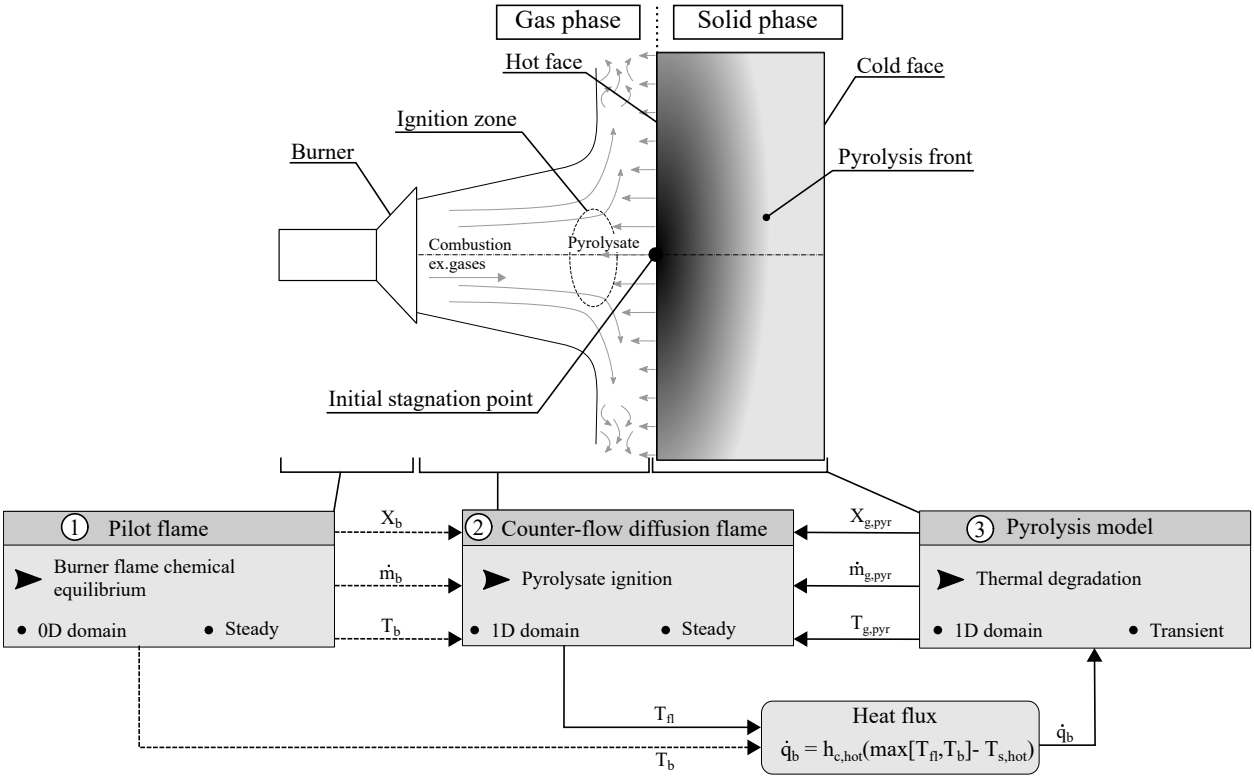

Figure 2: Architecture of the coupled approach, which consists of three sub-models coupled together. The temperature and composition of the pilot flame impinging on the composite are modeled in zero-dimension at stationary state with Cantera (sub-model 1). The pyrolysate composition, mass flow rate and temperature are computed with a one-dimensional transient pyrolysis model (sub-model 2). The mixing of pyrolysate with pilot flame exhaust gases and their ignition are modeled with a one-dimensional stationary counterflow diffusion flame model in Cantera (sub-model 3). The arrows represent data fluxes. Dashed arrows depict weak coupling (variables computed only once) and solid arrows depict strong coupling (variables updated at each iteration).

Species	N	CO_2	O_2	H_2O
Molar composition (−)	0.57	0.19	0.15	0.076

Table 2: Composition of the exhaust gases emitted by the partially premixed methane burner used in the small-scale fire test. Only the main species ($\geq 0.07\ \mathrm{mol\,mol^{-1}}$) are reported here.

4.3. Counterflow diffusion flame modeling (sub-model 2)

The counterflow diffusion flame model provided by Cantera [30] (class *CounterflowDiffusionFlame* in Python) is used to calculate the pyrolysate ignition. Three boundary conditions were defined on each side: the mass flow rate $\dot{m}_b$, temperature T_b and composition X_b of the exhaust gases on the burner side, and the pyrolysate mass flow rate $\dot{m}_{g,pyr}$, temperature $T_{g,pyr}$ and composition $X_{g,pyr}$ on the material side. The calculation of the temperature profile is then performed in a one-dimensional domain going from the burner exit to the material surface. Material ignition is defined here as the moment at which the boundary layer temperature exceeds the temperature of the exhaust gases of the pilot flame. This is a practical criterion as the objective of this study is to determine when the heat feedback from pyrolysate ignition outreaches the heat flux provided by the calibrated pilot flame. This sub-model is based on a well-known solver (Cantera) which has been validated independently in similar configurations involving counterflow diffusion flame [55–57].

4.4. Solid phase modeling (sub-model 3)

This section aims at developing a generalized and comprehensive pyrolysis model. First, the multi-components approach used to compute the composite properties as a function of the properties of its phases is introduced, and the modeling of the decomposition rate is described. Then, a mathematical model based on conservation equations is developed. Finally, the finite element formulation and time-step integration are introduced. The model is based on the following assumptions:

- The control volume remains constant, which implies that the variation of mass and density are equivalent. Swelling and delamination are neglected [16].
- The gas behave accordingly to the perfect gas law [8].
- The entire void space contained in the composite, i.e. its pores, is interconnected [58].
- The diffusivity D ($\mathrm{m^2\,s^{-1}}$) is assumed to be the same for all gaseous species and equal to their kinematic viscosity ν ($\mathrm{m^2\,s^{-1}}$) [8].

- The pyrolysate vapors are assumed to be in thermal equilibrium with the solid phase [59] and flow toward the hot face through the porous media with no resistance [53, 60]. Gas migration toward the cold face is not modeled, since the cold face is considered impermeable until the matrix is consumed. The Darcy law could alternatively be used to model pressure build-up and gas migration in both directions, but it requires the measurement and modeling of the composite permeability, which has not been done in this work.

- Heat is assumed to be transmitted from the pilot flame to the composite by convective heat transfer only, and radiative heat transfer from the flame is neglected. Flames involve four types of heat transfer mechanisms (convection, thermochemical heat release, radiation and water vapor condensation), but forced convection has been identified as the main heat transfer in flame impingement configurations, typically 70-90% for flame temperatures up to 1700 K [61], above the temperature of the pilot flame in this work (1366 K).

- The convective heat transfer coefficient is assumed to remain constant during the entire fire test, even after emission of pyrolysate on the hot face of the solid, because the mass flow rate of pyrolysate is expected to be much lower than the mass flow rate of exhaust gases from the pilot flame. Further work is needed to investigate how the formation of a diffusion flame in the boundary layer would affect the convection coefficient, for instance with CFD simulations. The convective heat transfer coefficient could alternatively be estimated with correlations as a function of the geometry of the impinging flame [62, 63], but most of these correlations are valid only for the idealized limiting case of an axisymmetric laminar stagnation flow on an infinitely extended plane, which is far from the situation encountered here.

4.4.1. Multi-components approach

A composite material undergoing thermal decomposition is composed of several distinct porous media, in the sense that every small volume at the mesoscopic level always contains both solid and gas phases, in the form of a solid component with an interconnected network of pores [58, 64]. Figure 3 presents a conceptual view of a control volume containing matrix, fibers, char and porosity, for a carbon/epoxy composite exposed to fire. The volume fraction X_i of each phase i is given by:

$$X_i = \frac{V_i}{V_{tot}} \tag{4}$$

where V_i is the volume of phase i and V_{tot} the total control volume. The volume fraction can be defined not only with respect to the control volume but also with respect to the total solid or gaseous phases as:

$$X_{i,p} = \frac{V_i}{\sum_{i=1}^{N_p} V_i} \tag{5}$$

where p represents the phase of interest ($p = s$ and $p = g$ for solid and gaseous phases, respectively) and N_p indicates the total number of solid or gaseous phases in the control volume. A distinction must be made between the *absolute* density ρ_i, that is the density of a control volume containing only the phase i, and the *weighted bulk* or *effective* density $\bar{\rho}_i$, that is the density of phase i with respect to a control volume containing several different phases. These quantities are related to each other as

$$\bar{\rho}_i = \rho_i X_i \tag{6}$$

Next, parameters with an overbar indicate *effective* quantities, defined with respect to the control volume. The total density of the control volume $\bar{\rho}$ is given by:

$$\bar{\rho} = \sum_{i=1}^{N} \bar{\rho}_i = \sum_{i=1}^{N} X_i \rho_i \tag{7}$$

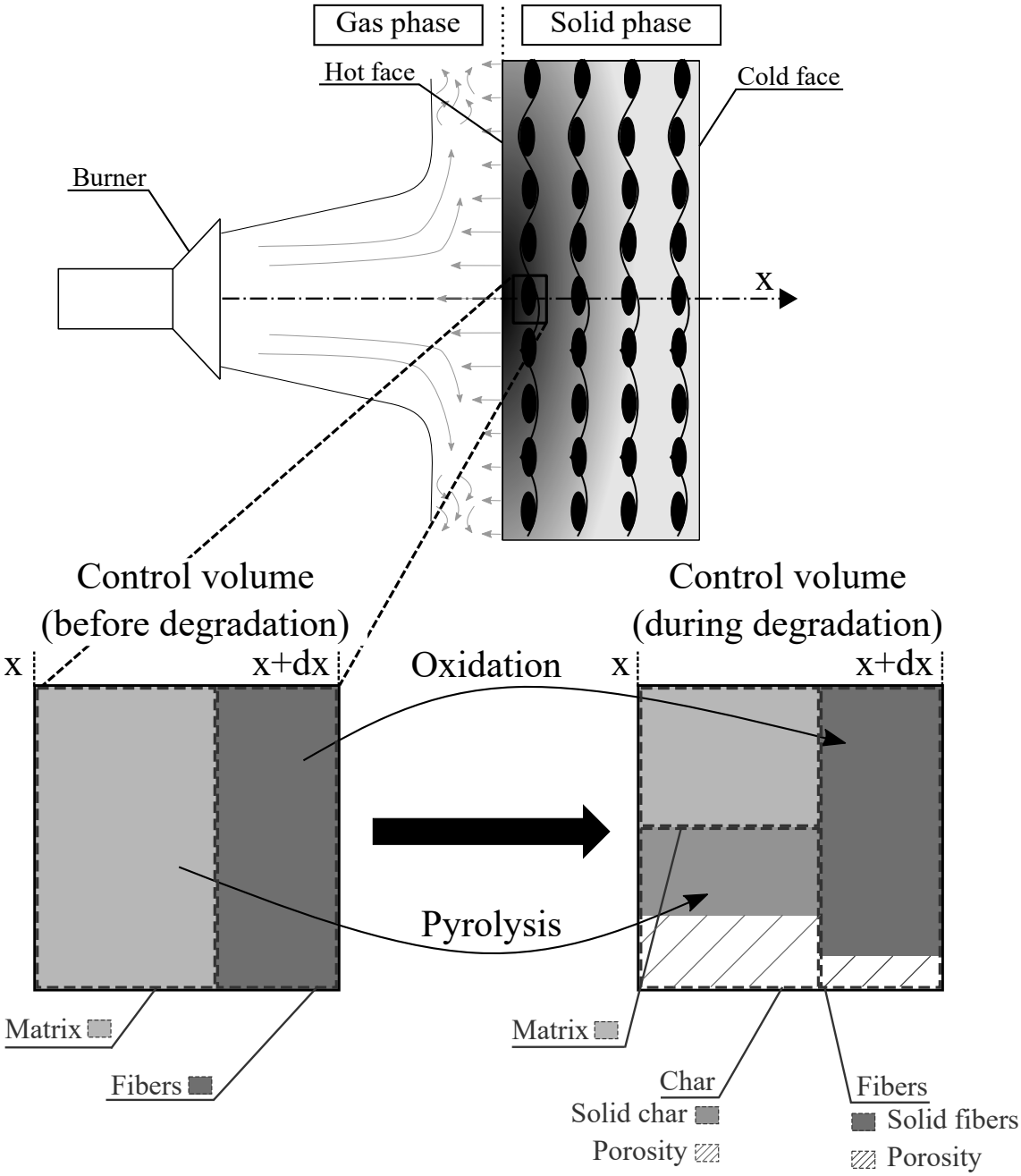

Figure 3: Illustration of a control volume containing several phases: matrix, char layer and carbon fibers. Although the domain is one-dimensional, the control volume has been drawn as a two-dimensional conceptual view for better understanding.

Then, the mass fraction is defined as:

$$Y_i = \frac{m_i}{m_{tot}} = \frac{\bar{\rho}_i}{\bar{\rho}} = X_i \frac{\rho_i}{\bar{\rho}} \tag{8}$$

The porosity represents the quantity of gas stored in pores appearing during the decomposition or initially present in the composite. It is defined as the volume fraction of void in each porous medium. The porosity ϕ_i ($\mathrm{m}^3\,\mathrm{m}^{-3}$) is computed from each species bulk density as:

$$\phi_i = 1 - \frac{\bar{\rho}_i}{\bar{\rho}_{i,0}} \tag{9}$$

where $\bar{\rho}_{i,0}$ corresponds to the effective density of the non-porous phase i over the control volume. Finally, the total porosity is given by:

$$\bar{\phi} = \sum_{i=1}^{N} X_i \phi_i \tag{10}$$

The temperature dependence of c_p and λ can be defined with a polynomial interpolation as:

$$\bar{\mathbb{P}}_i(T) = \sum_j C_{ij} T^j \tag{11}$$

where C_{ij} is the jth polynomial coefficient of the ith thermo-physical property. The parameters C_{ij} are then chosen empirically to fit experimental data representing the property $\bar{\mathbb{P}}_i$ as a function of temperature. Once the temperature-dependent properties of each phase have been calculated, the *effective* thermo-physical properties of the entire control volume can be computed with mass (c_p) or volume fraction (λ, ρ, ϕ, M, emissivity ϵ (-)).

4.4.2. Modeling of the decomposition rate

Consider a system of reactions composed of N_r equations including N_i different species, occurring in the sample during fire exposure

$$\sum_{i=1}^{N_i} \theta'_{ij} S_i = \sum_{i=1}^{N_i} \theta''_{ij} S_i + q_j \tag{12}$$

where the θ_{ij} are the mass stoichiometric coefficients and S_i the different species. The reaction rate k_j of each reaction j is computed according to:

$$k_j = (\bar{\rho}_0 - \bar{\rho}_\infty) \left[\frac{\bar{\rho} - \bar{\rho}_\infty}{\bar{\rho}_0 - \bar{\rho}_\infty} \right]^{n_j} A_j \exp\left(-\frac{E_j}{RT} \right) \tag{13}$$

where n_j is the reaction order and $\bar{\rho}_0$ and $\bar{\rho}_\infty$ respectively refer to the initial and final (after decomposition) densities of the reacting phase.

4.4.3. Mathematical model

The thermo-chemical model consists of simultaneously modeling the conservation of solid species, gas phase mass, gaseous species and energy in a one-dimensional domain:

$$\frac{\partial \bar{\rho}_i}{\partial t} = \sum_{j=1}^{N_r} \theta_{ij} k_j \tag{14a}$$

$$\frac{\partial \rho_g \bar{\phi}}{\partial t} + \frac{\partial \dot{m}_g}{\partial x} = \sum_{i=1}^{N_g} \sum_{j=1}^{N_r} \theta_{ij} k_j \tag{14b}$$

$$\bar{\phi} \rho_g \frac{\partial Y_{i,g}}{\partial t} + \dot{m}_g \frac{\partial Y_{i,g}}{\partial x} = \frac{\partial}{\partial x} \left(\bar{\phi} \rho_g D \frac{\partial Y_{i,g}}{\partial x} \right) + \sum_{j=1}^{N_r} \theta_{ij} k_j \tag{14c}$$

$$\bar{\rho} \bar{c_p} \frac{\partial T}{\partial t} + \dot{m}_g \bar{c_{pg}} \frac{\partial T}{\partial x} = \frac{\partial}{\partial x} \left(\bar{\lambda} \frac{\partial T}{\partial x} \right) + \sum_{j=1}^{N_r} k_j q_j \tag{14d}$$

where N_r is the number of chemical reactions and ρ_g the gas density ($\mathrm{kg\,m^{-3}}$). As the material temperature increases, it also loses heat by radiation. The heat flux on the hot face of the material is given by:

$$j_{q,hot} = h_{c,hot}(T_{bl} - T_{hot}) - \sigma\epsilon_{hot}(T_{hot}^4 - T_0^4) \tag{15}$$

where $h_{c,hot}$ is the convective heat transfer coefficient between the pilot flame and the solid surface ($\mathrm{W\,K^{-1}\,m^{-2}}$), σ the Stefan-Boltzmann constant ($\mathrm{W\,m^{-2}\,K^{-4}}$) and T_{hot} the hot face temperature. T_0 is the temperature of the surroundings and also the initial material temperature. The heat flux measurement with a heat gauge on the composite surface yields $h_{c,hot} = 108.5\ \mathrm{W\,m^{-2}\,K^{-1}}$ close to the stagnation point. In this work, the material emissivity ϵ_{hot} is assumed to be 0.85, which corresponds to an average value of the emissivities measured for various carbon/epoxy composites found in another work [65]. T_{bl} denotes the temperature immediately outside of the boundary layer in the gas phase close to the composite hot surface. The key concept of this coupled approach is to use different values of T_{bl} over time. At the beginning of the fire test, when the pyrolysate flow is not significant, T_{bl} is equal to the pilot flame temperature T_b. The effective temperature for the heat transfer across the boundary layer next to the sample surface T_{bl} is then taken as the highest temperature between T_b and the temperature computed by the counterflow diffusion flame sub-model T_{fl}. The radiative heat feedback from the pyrolysate ignition is neglected, when compared to the convective heat transfer from the impinging flame. On the cold face, the material is assumed to be subjected to natural convection and radiation heat losses such that:

$$j_{q,cold} = -h_{c,cold}(T_{cold} - T_0) - \sigma\epsilon_{cold}(T_{cold}^4 - T_0^4) \tag{16}$$

where $h_{c,cold}$ and T_{cold} are respectively the convection coefficient and material temperature on the cold face. $h_{c,cold}$ is computed with the McAdams correlation for natural convection [66]. The initial density of the gaseous species in the solid, as well as the initial flux of gaseous

species on each boundary, are set to zero. The mass flow rate $\dot{m}_g$ is computed by integrating Equation 14b:

$$\dot{m}_g = \int_{x_{cv}}^{L} \left(\sum_{i=1}^{N_g} \sum_{j=1}^{N_r} \theta_{ij} k_j - \frac{\partial \rho_g \bar{\phi}}{\partial t} \right) dx \tag{17}$$

where L is the composite thickness. By analogy with heat transfers, Robin boundary conditions are assumed on each face to compute the mass fraction $Y_{i,g}$ as:

$$j_Y = \frac{h_c}{\bar{c}_{pg}} \left(Y_{i,g}|_{\infty} - Y_{i,g} \right) \tag{18}$$

4.4.4. Finite Element Formulation

The system of coupled differential equations 14a to 14d is modeled with the Finite Element approach [67]. The temperature $T(x,t)$ and mass fractions $Y_{i,g}$ are discretized over the entire computational domain, divided into n elements. Each element is constituted of two nodes to which a value of T and $Y_{i,g}$ are assigned. In the following, a simple bar under a letter indicates a vector and a double bar a matrix. Between two nodes, the variables are approximated on each element Ω^e by a linear interpolation represented by an approximation function $\underline{\boldsymbol{\psi}}^e(x)$ as:

$$T(x,t) = \underline{\boldsymbol{\psi}}^e(x) \underline{\boldsymbol{T}}^e(t) = \sum_{j=1}^{2} \psi_j^e(x) T_j^e(t) \tag{19}$$

$$Y_{i,g}(x,t) = \underline{\boldsymbol{\psi}}^e(x) \underline{\boldsymbol{Y}}_{i,g}^e(t) = \sum_{j=1}^{2} \psi_j^e(x) Y_{ij,g}^e(t) \tag{20}$$

with:

$$\underline{\boldsymbol{\psi}}^e(x) = \begin{bmatrix} \frac{l-x}{l} & \frac{x}{l} \end{bmatrix} \tag{21a}$$

$$\frac{\partial \underline{\boldsymbol{\psi}}^e(x)}{\partial x} = \begin{bmatrix} \frac{-1}{l} & \frac{1}{l} \end{bmatrix} \tag{21b}$$

where l is the length of one element (m). The Bubnov-Galerkin method is applied to Equations 14c and 14d and all the terms are regrouped [67], providing the *finite element model*:

$$\underline{\underline{\boldsymbol{C}}}_Y^e \underline{\dot{\boldsymbol{Y}}}_{i,g}^e + (\underline{\underline{\boldsymbol{K}}}_{Y,1}^e + \underline{\underline{\boldsymbol{K}}}_{Y,2}^e)\underline{\boldsymbol{Y}}_{i,g}^e = \underline{\boldsymbol{F}}_{Y,1}^e - \underline{\boldsymbol{F}}_{Y,2}^e \tag{22}$$

With:

$$\underline{\underline{\boldsymbol{C}}}_Y^e = \int_0^l \underline{\boldsymbol{\psi}}^{eT} \bar{\phi}^e \rho_g^e \underline{\boldsymbol{\psi}}^e \, dx \tag{23a}$$

$$\underline{\underline{\boldsymbol{K}}}_{Y,1}^e = \int_0^l \underline{\boldsymbol{\psi}}^{eT} \dot{m}_g^e \frac{\partial \underline{\boldsymbol{\psi}}^e}{\partial x} \, dx \tag{23b}$$

$$\underline{\underline{\boldsymbol{K}}}_{Y,2}^e = \int_0^l \frac{\partial \underline{\boldsymbol{\psi}}^{eT}}{\partial x} \bar{\phi}^e \rho_g^e D^e \frac{\partial \underline{\boldsymbol{\psi}}^e}{\partial x} \, dx \tag{23c}$$

$$\underline{\boldsymbol{F}}_{Y,1}^e = \begin{bmatrix} -j_{Y,0} \\ j_{Y,l} \end{bmatrix} \tag{23d}$$

$$\underline{\boldsymbol{F}}_{Y,2}^e = \int_0^l \underline{\boldsymbol{\psi}}^{eT} \sum_{j=1}^{N_r} \theta_{ij} k_j \, dx \tag{23e}$$

$$\underline{\underline{\boldsymbol{C}}}_T^e \underline{\dot{\boldsymbol{T}}}^e + (\underline{\underline{\boldsymbol{K}}}_{T,1}^e + \underline{\underline{\boldsymbol{K}}}_{T,2}^e)\underline{\boldsymbol{T}}^e = \underline{\boldsymbol{F}}_{T,1}^e - \underline{\boldsymbol{F}}_{T,2}^e \tag{24}$$

With:

$$\underline{\underline{\boldsymbol{C}}}_T^e = \int_0^l \underline{\boldsymbol{\psi}}^{eT} \bar{\rho}^e \bar{c}_p^e \underline{\boldsymbol{\psi}}^e \, dx \tag{25a}$$

$$\underline{\underline{\boldsymbol{K}}}_{T,1}^e = \int_0^l \underline{\boldsymbol{\psi}}^{eT} \dot{m}_g^e \bar{c}_{p,g}^e \frac{\partial \underline{\boldsymbol{\psi}}^e}{\partial x} \, dx \tag{25b}$$

$$\underline{\underline{\boldsymbol{K}}}_{T,2}^e = \int_0^l \frac{\partial \underline{\boldsymbol{\psi}}^{eT}}{\partial x} \bar{\lambda}^e \frac{\partial \underline{\boldsymbol{\psi}}^e}{\partial x} \, dx \tag{25c}$$

$$\underline{\boldsymbol{F}}_{T,1}^e = \begin{bmatrix} -j_{q,0} \\ j_{q,l} \end{bmatrix} \tag{25d}$$

$$\underline{\boldsymbol{F}}_{T,2}^e = \int_0^l \underline{\boldsymbol{\psi}}^{eT} \sum_{j=1}^{N_r} k_j q_j \, dx \tag{25e}$$

Finally, the elemental matrices are assembled to calculate the global matrices [67]. It is worth noting that the element matrices $\underline{\underline{\boldsymbol{C}}}$, $\underline{\underline{\boldsymbol{K}}}$ and $\underline{\boldsymbol{F}}$ depend on the element properties, which in turn depend most of time on the variables Y and T. Therefore, their terms are computed with estimated variables and the convergence is investigated in an iterative process with the fixed point method.

The duration of the fire test is divided into m discrete time steps and the duration of an interval is $\Delta t = t^{n+1} - t^n$, where n indicates the time step number. The variation of T in one time step is described by the Crank-Nicholson approach [67]:

$$\frac{\partial \underline{\boldsymbol{T}}^a}{\partial t} = \frac{\underline{\boldsymbol{T}}^{n+1} - \underline{\boldsymbol{T}}^n}{\Delta t} \tag{26a}$$

$$\underline{\boldsymbol{T}}^a = (1 - \Theta)\underline{\boldsymbol{T}}^n + \Theta \underline{\boldsymbol{T}}^{n+1} \tag{26b}$$

where the superscript a denotes the approximation of T used to compute the element matrices and $\Theta = 0.5$. A similar procedure is used to compute the temporal variation of $Y_{i,g}$. Finally, Figure 4 represents the code algorithm.

4.4.5. Model validation

For validation purposes, the sub-model 3 has been used to reproduce the results of another work from Looyeh *et al.* [60], in which a 10.9 mm thick polyester-based composite reinforced with 45% of glass fibers is exposed to a furnace heating on its hot face and insulated on the cold face. The code formalism has been slightly adapted to adequately represent the equations introduced in [60]. The effect of the furnace is accounted for by a time-dependent Dirichlet boundary condition on the hot face and the materials properties are given in [60]. It is worth noting that the value of the heat of decomposition from polyester pyrolysis indicated in [60] (2.3446×10^5 J kg^{-1}) is different from the value indicated in subsequent articles using the same material [68–70] (2.3446×10^6 J kg^{-1}); therefore, the second value has been used in this article. Moreover, as pointed out by Krysl *et al.* [71], the modeling of the thermal

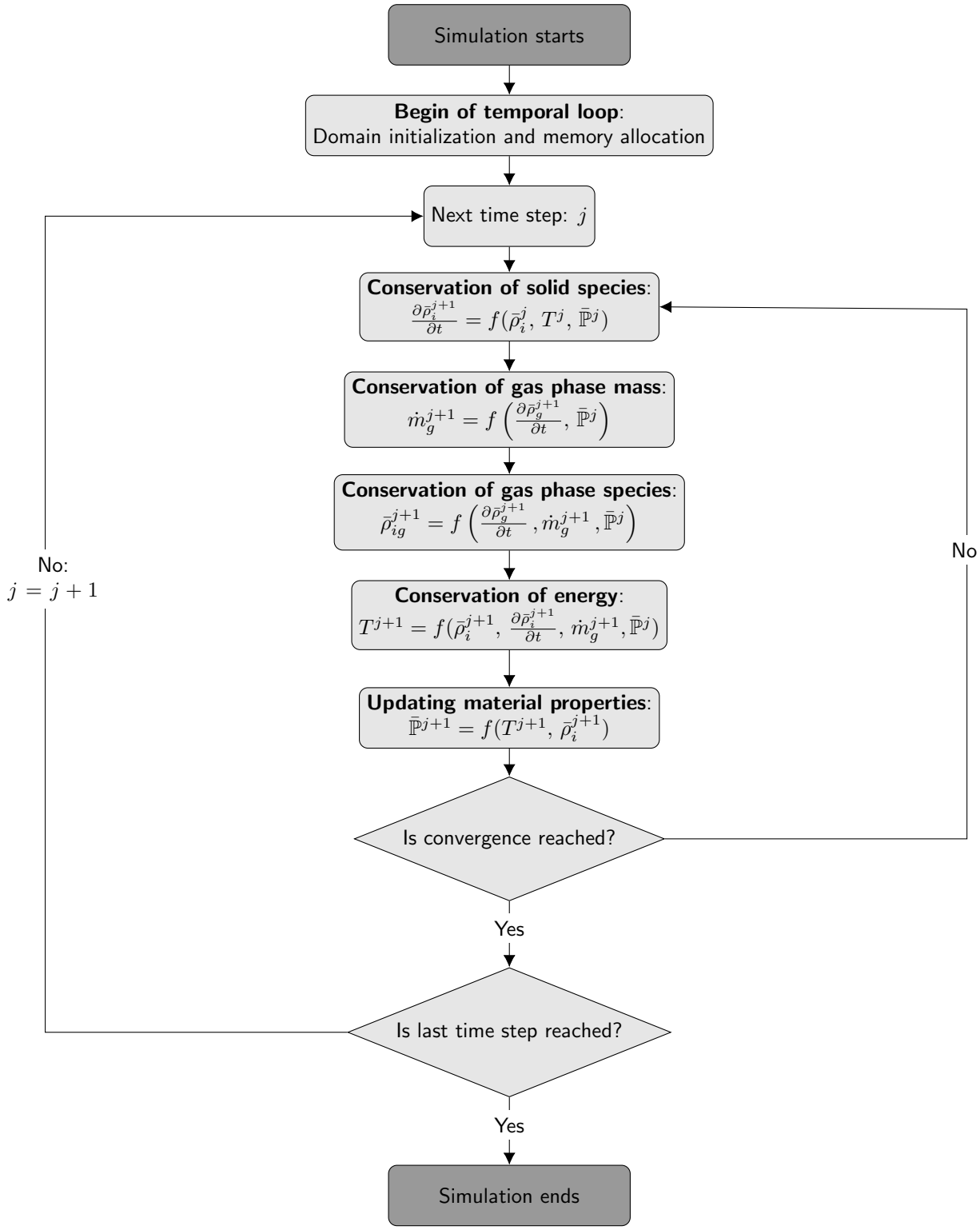

Figure 4: Algorithm representing the simulation steps.

properties of the degraded material are unclear in [60]. Figure 5 below shows a comparison between experimentally measured and predicted temperature profile of the material as a function of time, at three different location along the thickness: 1/10 of the thickness, 5/10 of the thickness and on the cold face. Figure 5 shows that sub-model 3 is able to predict the variation of the material temperature, except after 800 s where the error increases, mostly because the thermal properties of the degraded material have not been clearly indicated in [60] as mentioned above. Nevertheless, these results validate the approach of sub-model 3.

5. Material characterization

An aerospace-grade carbon-fiber epoxy pre-preg (procured from Solvay - formerly CYTEC - Tulsa, OK, USA) was selected as the base material to apply the proposed approach. This material system (carbon reinforcement: HTS40 E13 3K PW) is based on an Out-of-Autoclave (OOA) toughened epoxy. An 8-ply quasi-isotropic laminate $[0°, +45°, 0°, -45°]_S$ was prepared following the manufacturer's recommended cure and post-cure cycles.

5.1. Physical properties

Both solid and gaseous species co-exist in the sample exposed to fire, as the decomposition degree progresses. The different phases making up the material are referred to here by the index m for the matrix, f for the fibers, ch for the char and g for the gaseous species (pyrolysis and oxidation products, air, combustion exhaust gases, etc).

At least two samples of the same material are required for a full characterization of the phases: a virgin composite sample (containing only matrix and fibers) and a fully pyrolyzed composite sample (containing only char and fibers). To prepare the fully pyrolysed sample, a virgin composite was placed into a furnace tube (Carbolite Gero STF) with an inert argon flow. The sample was then heated at 3 K/min until reaching 1300 K, then kept at a constant temperature for one hour. The mass of the samples was reduced by 26.5% $\pm$ 0.43% after pyrolyzation. With this method, the fully pyrolyzed sample contained only non-oxidized

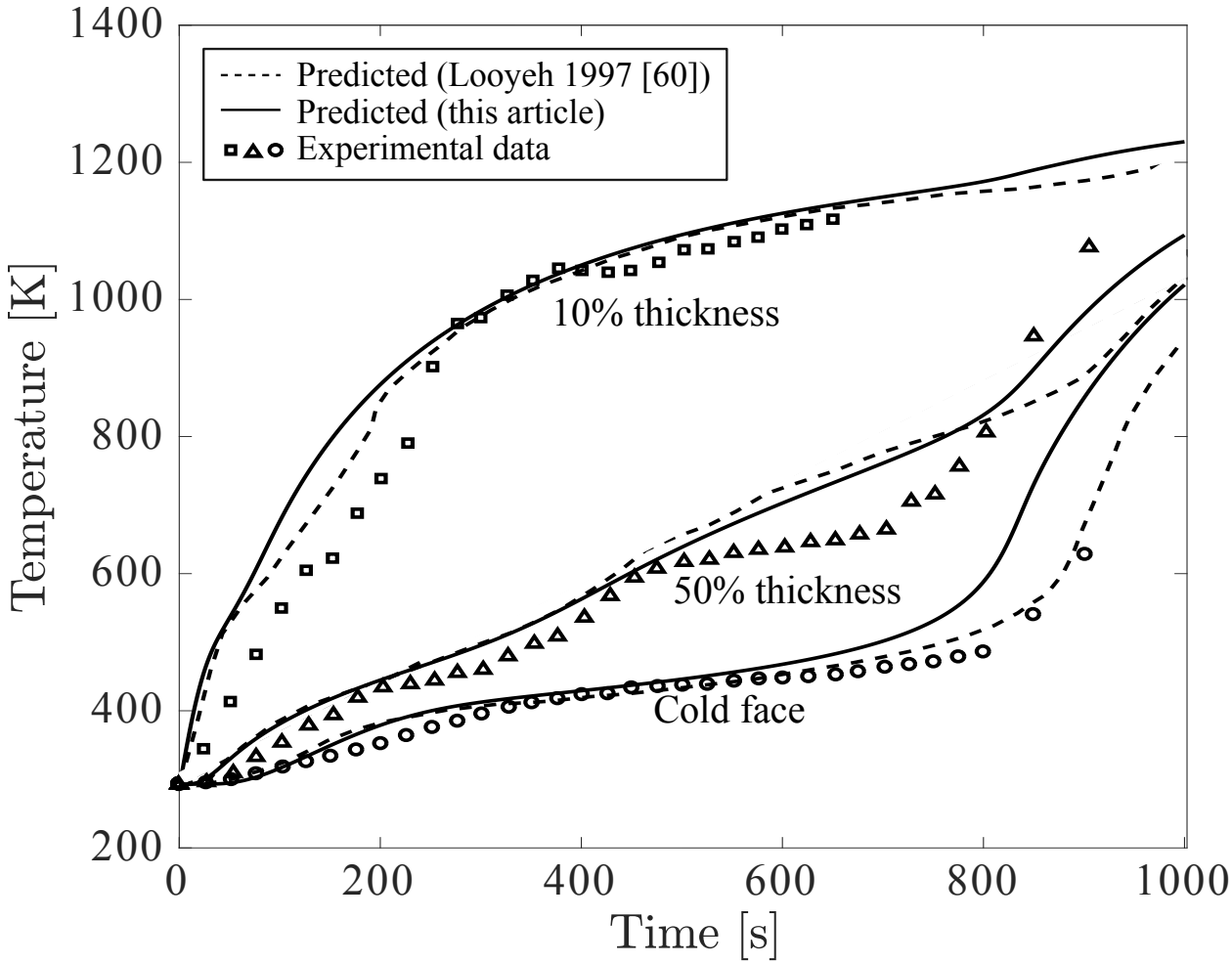

Figure 5: Comparison of experimental and predicted temperature profile through the thickness of a polyester-based glass reinforced composite of 10.9 mm thickness, exposed to a furnace test on the hot face and insulated on the cold face [60]. The dashed lines depict the temperature predicted by Looyeh *et al.* [60] and the continuous lines depict the temperature predicted with the code developed in this article. The squares, triangles and circles represent experimental data obtained from thermocouples placed at respectively 1/10 of the thickness, 5/10 of the thickness and on the cold face of the material.

Phase	ρ_i ($\mathrm{kg\,m^{-3}}$)	Virgin sample		Pyrolyzed sample	
		$X_{i,v}$ ($\mathrm{m^3/m^3}$)	$Y_{i,v}$ (kg/kg)	$X_{i,p}$ ($\mathrm{m^3/m^3}$)	$Y_{i,p}$ (kg/kg)
Matrix	1180 [72]	0.5168	0.4176	-	-
Fibers	1760 [72]	0.4832	0.5824	0.4832	0.7924
Char	1488.7 [12]	-	-	0.1494	0.2073
Pyrolysates	1.017 [12]	-	-	0.3674	3.480×10^{-4}

Table 3: Physical properties of the carbon/epoxy composite.

fibers and char. The density of a virgin sample was measured using the Archimedean principle at 297.65 K (24.5 °C). This method yielded a density for the virgin composite of $\rho_v = 1460.27 \pm 1.5\%\ \mathrm{kg\,m^{-3}}$, where the index v refers to a virgin sample. The density of the pyrolyzed composite was computed using the mass loss previously measured and assuming constant volume, yielding $\rho_p = 1073.3\ \mathrm{kg\,m^{-3}}$, where the index p refers to a pyrolyzed sample. For each sample, the composite density is expressed as a function of the phase densities and volume fraction as:

$$\bar{\rho}_v = X_m\rho_m + X_f\rho_f = \bar{\rho}_m + \bar{\rho}_f \tag{27}$$

$$\bar{\rho}_p = X_m[\phi_{ch}\rho_g + (1-\phi_{ch})\rho_{ch}] + X_f\rho_f \tag{28}$$

Considering the matrix and fiber densities provided by the material supplier and neglecting the porosity of the virgin composite, the matrix and fiber volume fractions can be obtained through Equation 27 and are listed in Table 3. Similarly, Equation 28 can be used to estimate the porosity if ρ_{ch} is known, which is crucial for calculating the thermal conductivity. However, the char density is challenging to measure independently. For this reason, the char density of another epoxy resin (M21, Hexcel) measured by Biasi [12] is used in the following to compute ϕ_{ch}.

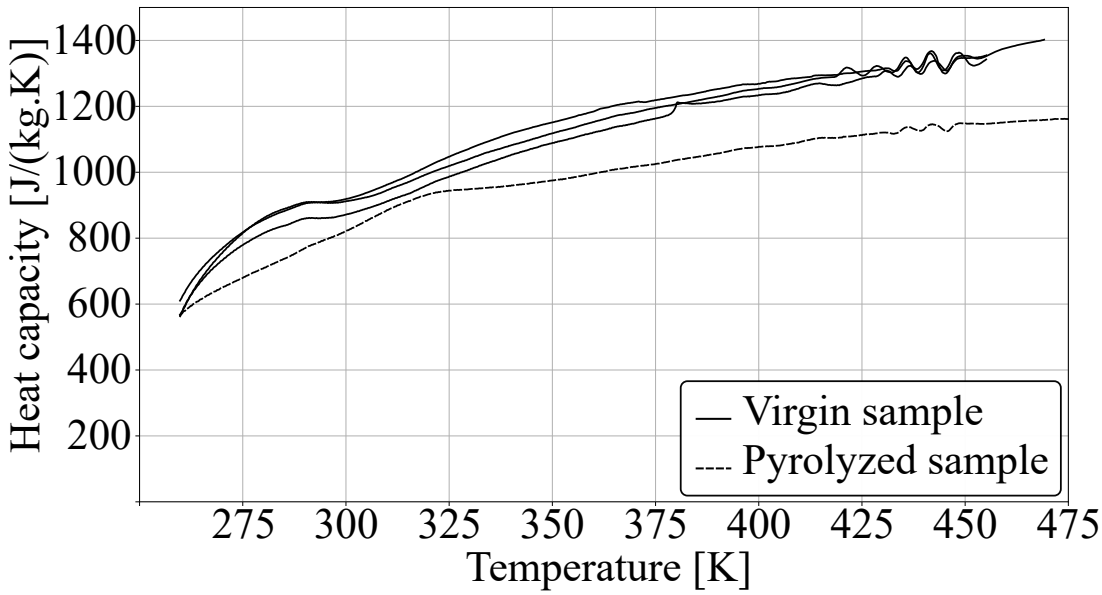

Figure 6: Heat capacity of the virgin and pyrolyzed carbon/epoxy obtained by DSC.

5.2. Thermal properties

5.2.1. Heat capacity

Figure 6 represents the heat capacities of the virgin and pyrolyzed samples measured by DSC (NETZSCH DSC 204F1 Phoenix) from 260 to 475 K. The heat flow of the samples was compared to that of a sapphire sample with similar mass and diameter, under inert atmosphere and at a heating rate of 20 K min^{-1}. The composite heat capacity was computed with a mixture rule weighed by the mass fraction of each phase. The determination of the heat capacity of each sub-phase from the global measurement requires the knowledge of thermal properties for at least one of the phases, for instance the carbon fibers which are common to both samples. To the best of our knowledge, the material system's reinforcement (HTS40 fiber) used in this work lacks publicly-available thermal properties. However, other polyacrylonitrile (PAN)-based commercial fibers have similar tensile strength and modulus. The AS4 carbon fibers which have been characterized between 280 and 680 K by other researchers [73], are used in this work. Considering these properties for the HTS40 carbon fibers, the matrix and char heat capacities can be determined from the DSC measurements carried out. Results and range of validity are shown in Table 4.

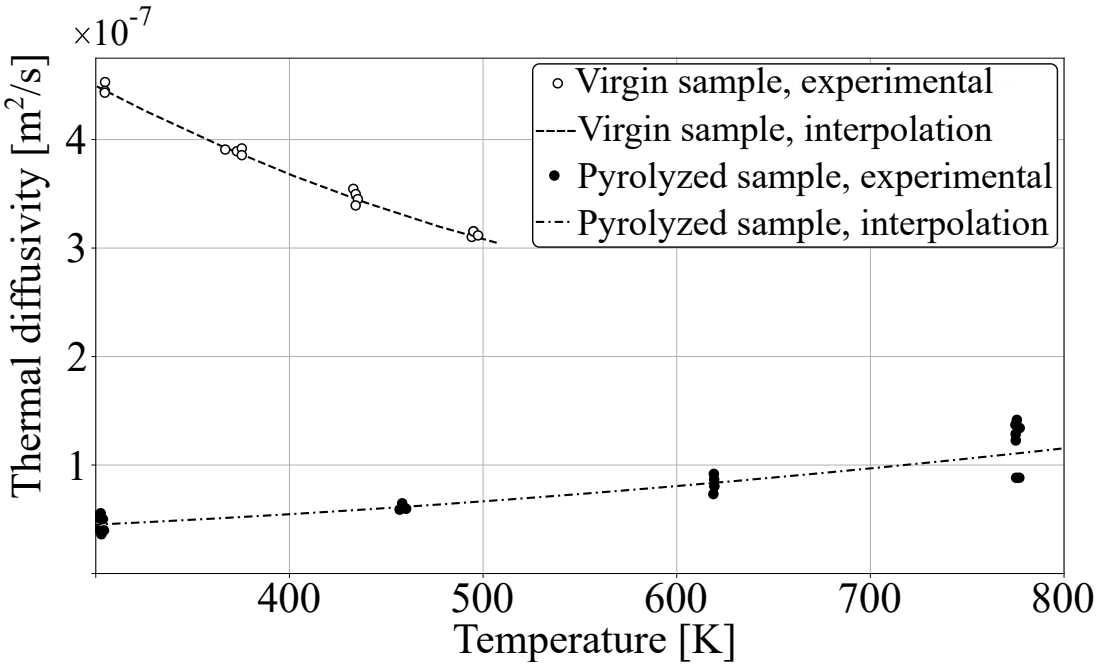

Figure 7: Thermal diffusivity of the virgin and pyrolyzed carbon/epoxy obtained by XFA. The dashed lines are polynomial interpolations.

5.2.2. Thermal conductivity

Figure 7 represents the material thermal diffusivity measured in vacuum with a Linseis XFA 600 system. The temperature programs ranged from 300 to 500 K, and 300 to 780 K for virgin and fully pyrolyzed samples, respectively. The thermal diffusivity of the fully pyrolyzed sample is lower than that of the virgin material, most likely because of the high level of porosity that hinders heat transfer.

The material conductivity is subsequently computed within an elementary control volume containing matrix, fibers, char and gas in three steps. First, the conductivity of the porous char layer $\lambda_{ch,porous}$ is computed as a function of the char and gas conductivities with the Maxwell's model [39]:

$$\lambda_{ch,porous} = \lambda_{ch} \left[\frac{\lambda_g + 2\lambda_{ch} + 2\phi_{ch}(\lambda_g - \lambda_{ch})}{\lambda_g + 2\lambda_{ch} - \phi_{ch}(\lambda_g - \lambda_{ch})} \right] \tag{29}$$

Then, the conductivity of the degraded matrix is computed as a function of the porous char and matrix conductivities with a rule of mixture following Reuss model, as the char is first

formed on the hot side of the control volume. A similar method is used to compute the conductivity of the oxidized fibers as a function of the fibers and gas conductivities as:

$$\lambda_{m,degr} = \left(\frac{X_m}{\lambda_m} + \frac{X_{ch,porous}}{\lambda_{ch,porous}}\right)^{-1} \tag{30}$$

$$\lambda_{f,degr} = \left(\frac{X_f}{\lambda_f} + \frac{\phi_f}{\lambda_g}\right)^{-1} \tag{31}$$

Finally, the conductivity of the complete composite is computed as a function of the degraded matrix and fibers conductivities with the Clayton model [40]:

$$\bar{\lambda} = \frac{\lambda_{m,degr}}{4}\left[\sqrt{(1-X_f)^2\left(\frac{\lambda_{f,degr}}{\lambda_{m,degr}}-1\right)^2 + \frac{4\lambda_{f,degr}}{\lambda_{m,degr}}} - (1-X_f)\left(\frac{\lambda_{f,degr}}{\lambda_{m,degr}}-1\right)\right]^2 \tag{32}$$

With a value for the thermal conductivity of the carbon fibers extracted from the literature, the thermal properties of all the phases are presented in Table 4. The radial thermal conductivity of the carbon fibers λ_f can be calculated from the axial one λ_{fa} with the orthotropy ratio $F = \lambda_{fa}/\lambda_f$ [74]. An orthotropy ratio of 6.10 has been estimated from the properties of a AS4/3501-6 carbon/epoxy composite [74], similar to the material used here.

5.3. Chemical properties

The kinetic triplet (A_j, E_j, n_j) describing reaction j in a thermal degradation model can be inferred experimentally from TGA measurements [75]. Carbon/epoxy samples were exposed to three different heating rates, i.e. 5, 10, and 25 $\mathrm{K\,min^{-1}}$, under inert (N_2) and oxidative atmospheres. The pilot flame releases several species, such as O_2, H_2O, CO_2, CO, O, OH that are likely to oxidize the carbon species contained in the composite. However, the exact composition of the exhaust gases from the pilot flame presented in Table 2 cannot be replicated in TGA experiments. For this reason, a standard method based on oxidation in air has been preferred in this work, following the procedures commonly used in the literature. Isoconversional methods were used to obtain the values of the kinetic triplet for matrix pyrolysis, char oxidation and fiber oxidation, assuming single-step decomposition [76]. The

Phase	$c_{p,i}$ ($\mathrm{J\,K^{-1}\,kg^{-1}}$)	Range (K)
Matrix	$-5156 + 30.68T$ $-0.0442T^2 + 2.071 \times 10^{-5}T^3$	260-475
Fibers	$2367 - 8.212T$ $+0.01615T^2 - 8.529 \times 10^{-6}T^3$	272-672 [73]
Char	$-1.219 \times 10^4 + 66.42T$ $-0.106T^2 + 5.302 \times 10^{-5}T^3$	260-475
Pyrolysates	$1972.5 + 1.45T$ $+9.59 \times 10^{-4}T^2 + 3.47 \times 10^{-7}T^3$	300-1000 [12]
Phase	λ_i ($\mathrm{W\,m^{-1}\,K^{-1}}$)	Range (K)
Matrix	$-1.1 + 9.084 \times 10^{-3}T$ $-1.838 \times 10^{-5}T^2 + 1.159 \times 10^{-8}T^3$	260-475
Fibers	$0.5638 + 0.002561T$	272-672 [73]
Char	$-0.08318 + 6.528 \times 10^{-4}T$ $-9.002 \times 10^{-7}T^2 + 7.662 \times 10^{-10}T^3$	300-800
Pyrolysates	$2.88 \times 10^{-2} + 7.74 \times 10^{-5}T$	300-1000 [12]

Table 4: Thermal properties of the carbon/epoxy composite determined from DSC and XFA experiments. Where a reference is provided, values were extracted from the literature for similar carbon fiber/epoxy composites.

parameters describing the chemical decomposition of the material are reported in Table 5, as well as the char yield θ_j ($\mathrm{kg\,kg^{-1}}$), that represents the quantity of char produced per kilogram of matrix pyrolyzed. Finally, the heat of reaction measured in [77] for an epoxy resin and in [12] for char and carbon fiber oxidation was used to quantify the heat absorbed or released by the material decomposition.

The outgassing from char and carbon fibers oxidation is assumed to be composed only of CO_2. The modeling of pyrolysate ignition being strongly influenced by their composition, more research is needed to measure quantitatively the composition of pyrolysate exhaust gases as a function of the material temperature and/or decomposition degree.

Reaction	E_j ($\mathrm{kJ\,mol^{-1}}$)	A_j ($\mathrm{s^{-1}}$)	n_j (-)	θ_j ($\mathrm{kg\,kg^{-1}}$)	q_j ($\mathrm{kJ\,g^{-1}}$)
Pyrolysis	193	2.20×10^{13}	3.03	0.3678	-2.5 [77]
Char oxidation	112	1.7×10^{4}	1.76	0	3.43 [12]
Fiber oxidation	260	4.93×10^{10}	4.83	0	8.94 [12]

Table 5: Reaction mechanism of a carbon/epoxy composite. Data inferred from TGA with different heating rates $5, 10, 25\ \mathrm{K\,min^{-1}}$.

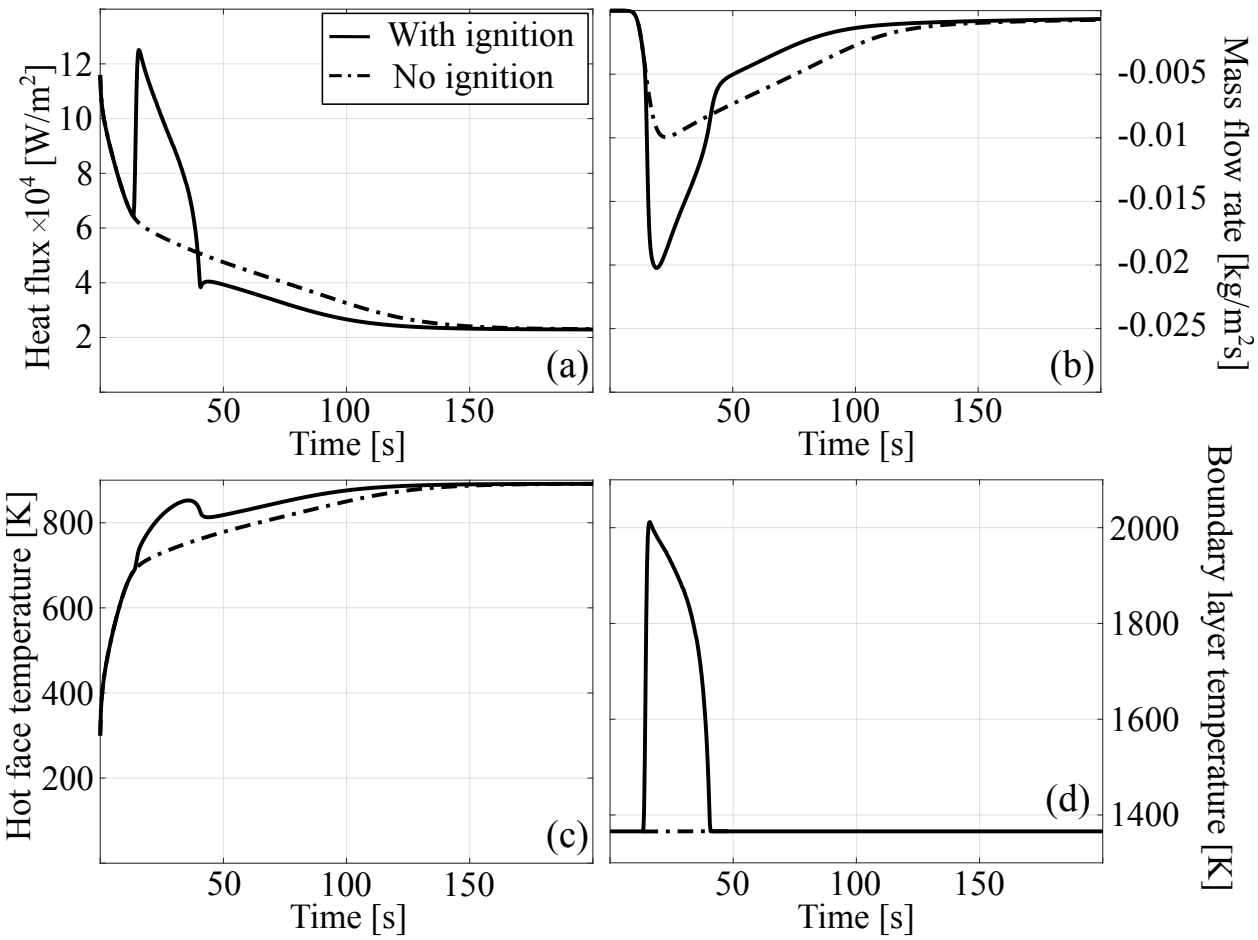

Figure 8: Temporal evolution of a) the heat flux received by the material on the hot face $j_{q,hot}$, b) the pyrolysate mass flow rate on the hot face $\dot{m}_{g,pyr}$, c) the hot face temperature $T_{g,pyr}$ and d) the boundary layer temperature T_{bl} close to the hot face.

6. Results and discussions

6.1. Gas phase reactions and heat feedback

The predictions of the model for the temporal evolution of the heat flux received by the material, the pyrolysate mass flow rate, the composite hot face temperature and the boundary layer temperature are shown in Figure 8. To assess the effect of pyrolysate ignition, two predictions are compared: a case with ignition, modeled with the coupled architecture introduced in Section 4.1, and a case without ignition, modeled with the pyrolysis model only (no coupling with Cantera). According to the results of Figure 8b), matrix pyrolysis and emissions of pyrolysates from the hot face starts after 8 seconds of fire exposure. Then, the pyrolysate mass flow increases with the matrix decomposition rate, until a critical value is reached corresponding to the ignition conditions in the boundary layer. After a flame exposure time of 14.1 s, the model predicts a boundary layer temperature that exceeds the pilot flame temperature. This threshold is selected as the criterion defining outgassing ignition, consistent with experimental observations of flames onset on the hot face of the composite after 9 to 11 s of fire exposure in our small-scale tests. After pyrolysate ignition, the heat flux received by the material increases by approximately 140%, increasing the material temperature and further promoting its degradation. At that point, a self-sustained combustion could be established; however, the formation of a porous layer of char mixed with carbon fiber and the endothermicity of the pyrolysis reduce greatly the heat transfer to the matrix remaining deeper in the sample. The pyrolysate mass flow rate starts to decrease after a flame exposure time of approximately 19 s, causing finally the flame extinction at approximately 41 s. The positive heat feedback from pyrolysate ignition is compensated after extinction, when compared to a case without ignition, by higher radiative heat losses and reduced convective heat transfer to the sample, again from the higher surface temperature. After 200 s, the hot face temperature is the same with and without pyrolysate ignition.

6.2. Solid phase degradation

Figure 9 shows the numerically predicted and experimentally measured evolution of the composite cold face temperature over a 600 s fire test, and Figure 10 presents the evolution calculated by our model for the composite temperature, density, porosity and diffusivity throughout its thickness, for different fire exposure times. For comparison purposes, a case without ignition has also been modeled and is shown on Figure 9. The initial exposure of the material to the flame, *i.e* between 0 and 11 s on Figure 9, corresponds to the heating of the material purely by conductive heat transfer within the solid phase, prior to thermal degradation onset. The variation of density at each time step provided in the model shows that the first significant variation of matrix density occurs close to $t = 11$ s. Figure 10b) shows that the matrix has already degraded significantly around $t = 15$ s and the mass loss is very rapid because of the high reactivity of the epoxy resin. As seen on Figure 8b), most of the pyrolysates are emitted between 14 and 40 s, leading to material ignition. Figures 8b) and 10b) show that the pyrolysis is complete after approximately 100 s, with the maximum temperature $T = 800$ K reached later on Figure 9, at $t = 166$ s. The temperature profile tends toward a steady state, slowly decreasing until the end of the certification test. This slow decrease can be explained by the reduction of the material thermal diffusivity because the carbon fiber and char oxidation increases the material porosity, as represented on Figure 10c) and 10d). This effect is especially important on the hot face of the material where the temperature is maximum, reducing the heat flux received from the flame.

6.3. Sensitivity Analysis

A sensitivity analysis was done to investigate the relative influence of input parameters variations on the pyrolysate combustion. In the solid phase, the material thermal diffusivity ($\mathrm{m^2\,s^{-1}}$), the kinetic triplet (E, A, n) and heat of reaction q describing the material pyrolysis have been varied by $\pm 30\%$. In the gas phase, the burner mass flow rate $\dot{m}_b$, mole fraction of O_2 in the exhaust gases from the pilot flame and mole fraction of fuel contained in the pyrolysate (H_2 and C_2H_2) are also varied by $\pm 30\%$. The relative proportions of the other

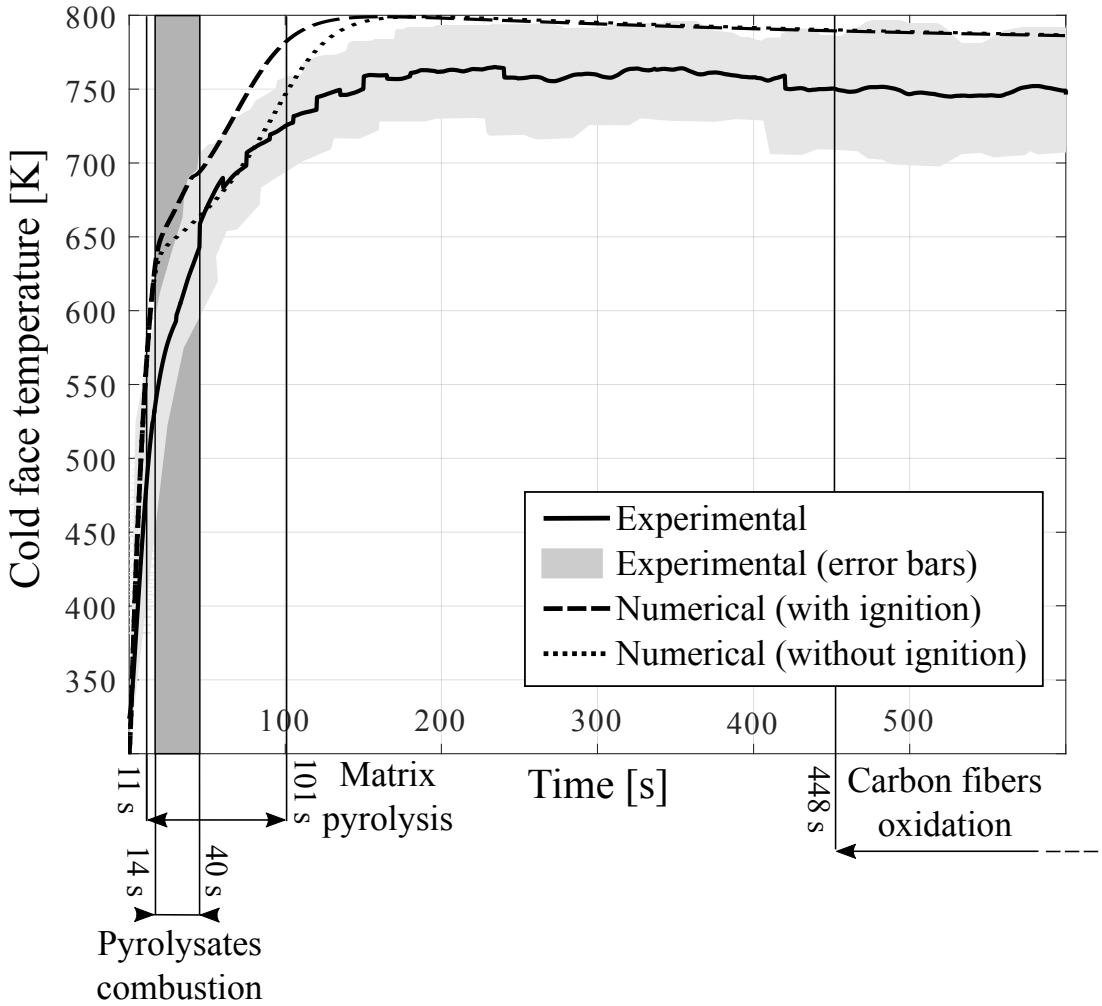

Figure 9: Numerical and experimental evolution over time of the composite back face temperature. The light grey zone shows the 95% Confidence Interval considering Student's t-distribution of experimental data. The dark grey zone represents the duration of pyrolysate combustion.

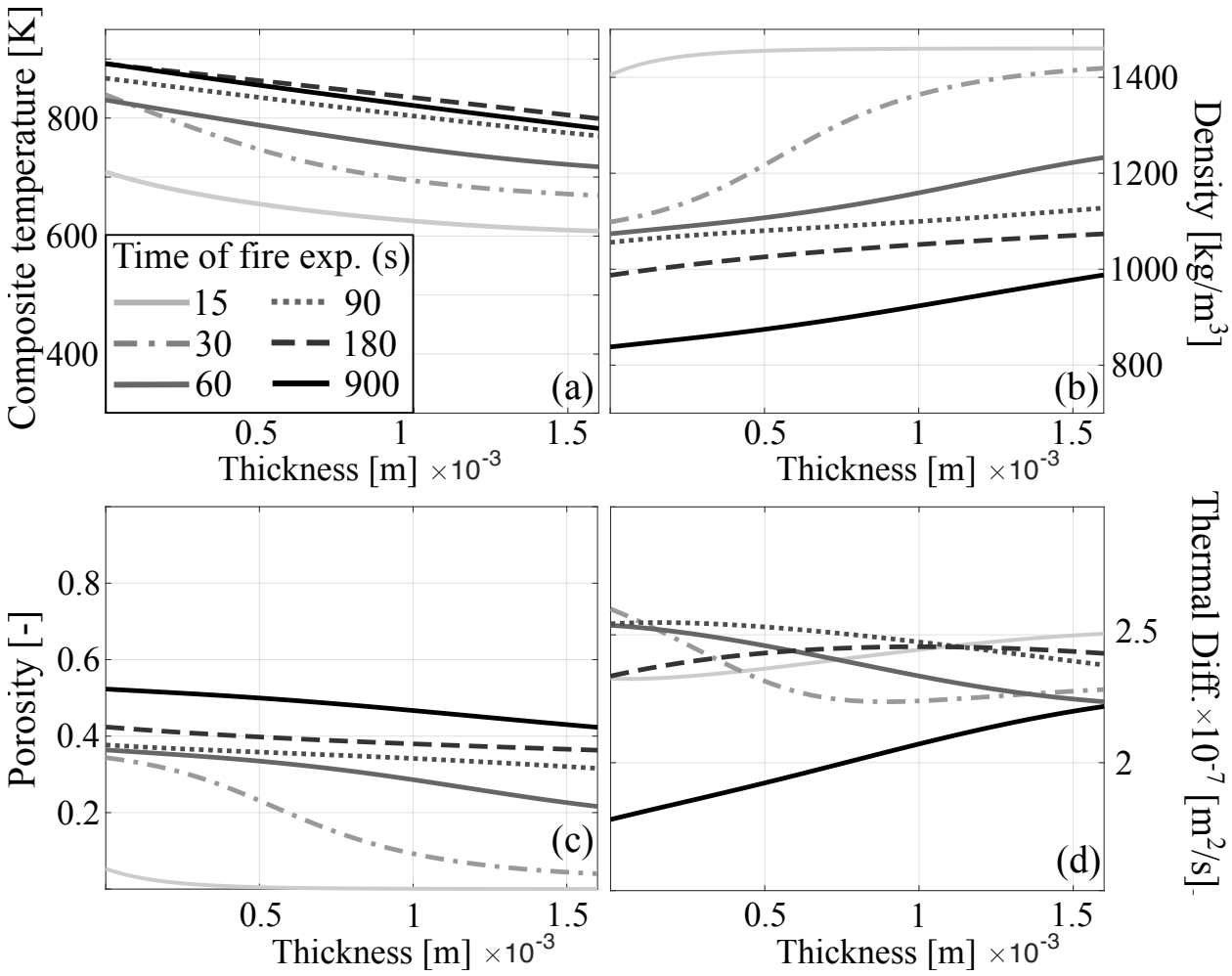

Figure 10: Prediction of the evolution over the thickness of the composite a) temperature, b) density, c) porosity and d) thermal diffusivity after 15, 30, 60, 90, 180 and 900 s of fire exposure.

species of Table 1 and 2 are kept constant. The variations of the time-to-ignition, maximum boundary layer temperature and maximum heat flux received by the material are reported in Figure 11.

In the solid phase, results show that the material thermal diffusivity has a relatively weak influence on the model response. A reduction of $\lambda/(\rho C_p)$ lessens the amount of heat transmitted to the material and therefore delays the onset of matrix pyrolysis, which explains why the time-to-ignition is slightly more important (+4.25%) when the diffusivity decreases. The effect on the boundary layer temperature is even more limited (−1.65%) and is bound to the hypothesis of local thermal equilibrium, which implies that the pyrolysate temperature is equal to the material hot face temperature. However, it appears that pyrolysate combustion is mainly driven by the activation energy (E) of the matrix pyrolysis. This parameter represents the amount of heat necessary to degrade the material and is therefore directly associated to the production of pyrolysates. A variation of +30% of E can totally prevent the ignition, and a deviation of −30% decreases the time-to-ignition by 75%. The effect on the boundary layer temperature and heat flux is less important, although still dominant when compared to the influence of other input parameters (+10% and +26%, respectively). Fluctuations in the char yield also have an impact on the three parameters describing the pyrolysate combustion, as it directly influences the quantity of pyrolysates produced by the pyrolysis. Therefore, a diminution of the char yield increases the mass flow rate of pyrolysates, reducing the time-to-ignition while increasing the heat feedback. This effect is however quite limited when compared to the impact of activation energy and gas-phase reactions.

The sensitivity analysis for the gas-phase reactions is especially valuable considering the high uncertainty in the model input data. A diminution of 30% of the fraction of fuel in pyrolysates and oxidizer in the pilot flame exhaust changes the time-to-ignition by +10.6% and −2.12%, respectively. These observations can be explained by considering that at the beginning of pyrolysis, the quantity of pyrolysate emitted in the environment is very low

when compared to the quantity of oxidizer available. Therefore, a reduction of the mole fraction of oxidizer or an augmentation of the mole fraction of fuel helps the mixture to reach its lower flammability limit. An increase of the fuel and oxidizer mole fractions promotes the heat feedback in similar proportions (+9%). An augmentation of the mass flow rate of exhaust gases increases the local velocity gradient (strain rate [78]) in the gas phase and therefore delays the time-to-ignition (+2.12%), although its effect is modest for all three parameters when compared to variations in pyrolysates or exhaust gases composition.

6.4. Discussions

The model slightly overestimates the material temperature during the fire test compared to experimental data, particularly during matrix pyrolysis. The origin of this error could not be clearly identified, because of the large number of processes interacting during pyrolysis. One likely explanation is however the swelling and delamination of the material, which are not considered in the model but observed in the experiments. The delamination process is a deconsolidation phenomenon of the fibrous structure, which is caused by the softening and subsequent decomposition of the matrix as well as the associated gas migration [5]. Moreover, the fiber crimp of woven architectures plays an important role in this process as it promotes spring-out. The presence of additional internal gas layers not considered in the model reduces again the heat transfer to the composite, which could explain the error observed during the fire test. However, it is worth noting that swelling is somewhat restrained in our case by the clamping of the sample on each extremity. Further work is required to model pressure build-up in the composite, for instance with the Darcy law to account for resistance to gas flow. The overestimation reaches 50 K at $t = 115$ s, which corresponds to an error of 6.7%, and increases at the later stages of the fire test. A better estimation of the heat released or absorbed by pyrolysis could also help to improve the agreement. Nevertheless, the qualitative agreement remains very good as the time to reach the maximum temperature and the overall shape of the curve are correctly predicted.

The temperature variation after the maximum has been reached at $t \approx 200$ s on Figure 9

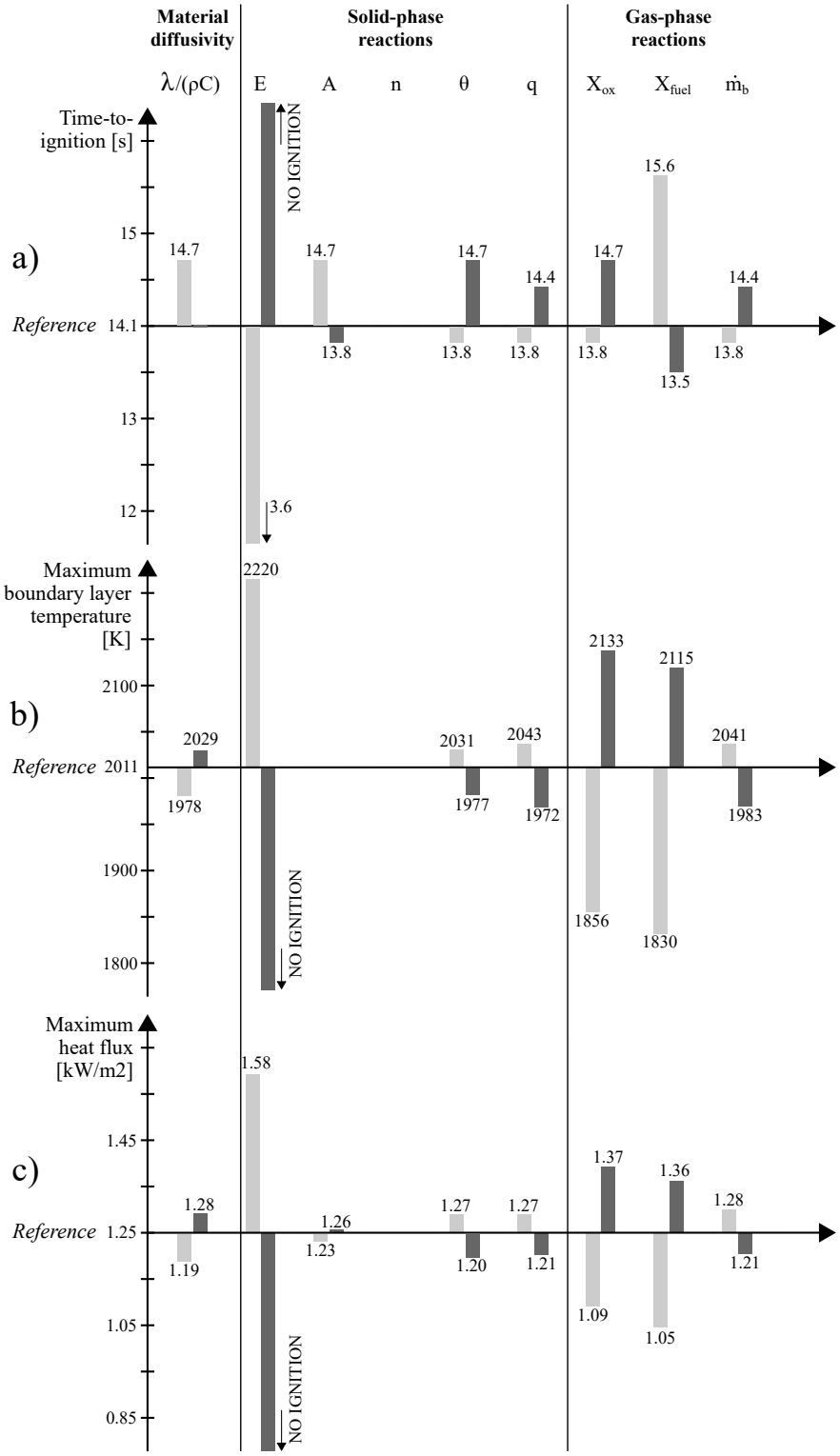

Figure 11: Effect of variations in input parameters (( ): −30%, ( ): +30%) to predict a) the time-to-ignition of pyrolysates, b) the maximum boundary layer temperature and c) the maximum heat feedback from pyrolysate combustion. The time-to-ignition has been predicted with a time-step of 0.3 s.

reveals that oxidation reactions are not negligible. Oxidation reactions are slow, when compared to other processes such as pyrolysis and swelling, which are completed once the steady state is reached. Therefore, the decrease of temperature observed experimentally on the cold face is likely to be due to a reduction of the thermal diffusivity on the hot face, from carbon fiber and char oxidation that increases porosity. However, oxidation reactions are most of the time neglected in previous models found in the literature [16, 17].

The error in temperature prediction with experimental data increases as the steady state is approached after 200 s, until reaching an overestimation of approximately 35 K at the end of the fire test (4.7% of the total temperature increase). This increased error is likely due to an underestimation of the carbon fiber oxidation. As a reminder, the composite oxidation has been characterized by TGA in an oxidative (air) atmosphere, containing approximately 20% of oxygen. However, the combustion exhaust gases of the pilot flame contain only 15% oxygen, but also contain H_2O, CO_2 and combustion radicals, notably OH, that can have a major impact on solid carbon oxidation [44]. The effect of such species is not considered in this work. The kinetic triplets characterizing graphite oxidation by these species have already been measured in the literature and could be adapted to epoxy-derived char and carbon fibers in a future work [79]. Results show that modeling the composite under fire test conditions using air flow-derived kinetic triplets is inaccurate, although it can provide a reasonable baseline in the absence of more appropriate source data.

It is also worth noting that the gases emitted by the fire test are evacuated by a ventilation system that can contribute to cooling the composite backface, as represented on Figure 1. This exhaust provides an additional weak forced convection term that has not been considered in the simulation results presented, in which the sample is cooled by natural convection only. Additional simulations have been done in this work with forced convection on the cold face and have shown that an air flow with a velocity of 1 $\mathrm{m\,s^{-1}}$ and at ambient temperature reduces the temperature overestimation at the end of the test to approximately 26 K, instead of 35 K, showing that the ventilation has a limited influence on the composite temperature.

A comparison between modeling with and without ignition reveals that ignition momentarily increases the material backface temperature, but this effect has vanished after 150 s. Although including pyrolysate ignition does not significantly change the backface temperature evolution on the long term, the heat feedback it yields to the sample is significant and the diffusion flame modeling approach implemented here provides a novel way to quantify it. During the time pyrolysate outgassing burns at the surface of the sample, the heat flux it receives approximately doubles, as shown in Figure 8a), an effect that should be considered when the temporal evolution of material properties or flame spread over the sample surface are of interest.

The comparison between numerical and experimental data reveals that this coupled approach is able to predict the time-to-ignition of a sample exposed to fire with good accuracy, without having to use optimization of material thermal properties against experimental data or empirical formulae. The time-to-ignition is slightly overestimated (14 s numerically versus 10 s experimentally), but this modeling is performed close to the stagnation point, where the strain rate can be very important because of the high radial velocity gradient of the exhaust gases from the burner. This could delay or even prevent the pyrolysate ignition [22]. The non-ignited pyrolysate could thus be advected away and may ignite at some radial distance away from the stagnation point, in locations with a lower strain rate and higher fuel concentration. A two-dimensional modeling of the same physical processes in both gas and solid phases would be required to investigate this phenomena.

However, the pyrolysate composition is considered constant during the fire test but in reality, the outgasses composition is temperature-dependent and most of the combustible gases are released at a specific pyrolysis temperature. This could also influence the prediction of the time-to-ignition. An independent modeling of each gaseous species with temperature-dependent source terms would allow to model a variable pyrolysate composition at the surface of the composite, providing more accurate results. However, the effect of such a modeling is expected to be quite limited as the pyrolysis is not homogeneous along the material thickness

because of temperature gradients. Nevertheless, the coupled modeling approach presented here, with detailed chemistry in the gas phase used to model ignition of the pyrolysate and heat feedback to the sample is comprehensive and can be extended by for instance variable outgassing composition or more detailed pyrolysis models in the solid phase.

Results from the sensitivity analysis show that pyrolysate combustion is mainly controlled by the activation energy of the matrix pyrolysis. However, variations of the composition of pyrolysates or exhaust gases from the pilot flame also have a significant effect on the gas-phase reactions. In particular, fluctuations in the mole fraction of oxygen in the exhaust gases affect both the time-to-ignition and heat feedback from pyrolysates combustion. Yet, the fraction of oxidizer contained in the flame exhaust is directly related to the burner operation parameters, such as the type of fuel and calibration method.

7. Conclusion

Pyrolysis models are used in the industry to predict the outcome of fire certification tests. Our results revealed that these predictive tools are very sensitive to the ignition of the pyrolysates emitted by the matrix decomposition, which provides an additional and non-controlled heat feedback at the surface of the material. Most of the time, the pyrolysate ignition is modeled with empirical parameters specific to each material and fire test conditions, or with simplified chemical kinetics that are not representative of the complexity of the processes at play. There is therefore a need to develop new theoretical approaches able to model the pyrolysate ignition regardless of the material or fire test conditions.

This research presents a new numerical approach to model the heat feedback and time-to-ignition at the surface of a composite exposed to fire test, that does not require empirical parameters specific to each test or material. This method relies on the coupling of several sub-models accounting for the thermal, chemical and physical processes in both gas and solid phases. The approach is implemented and compared against experimental data for a carbon fiber epoxy matrix composite, whose thermal, physical and chemical properties have

been measured experimentally through simple and standardized experiments (Archimedean principle, DSC, XFA and TGA). The comparison between modeling results and experimental data obtained in a small-scale fire test facility reproducing the conditions of certification demonstrates the ability of the model to predict the composite backface temperature with a maximal error of 6.7% (50 K) in realistic test conditions. In particular, the prediction of the time for increased heat release in the boundary layer due to pyrolysate ignition (14s in the model) is consistent with the time-to-ignition measured experimentally in the fire test ($9 - 11$s). Results also show that the heat flux received by the material increases by approximately 140% just after the onset of pyrolysate combustion, although such ignition is often neglected in the literature. However, pyrolysate ignition has no significant influence on the composite thermal degradation if the fire test lasts more than 200 s. A sensitivity analysis showed that uncertainty in the pyrolysate combustion is mainly affected by changes in the activation energy of the matrix pyrolysis, which indicates that this parameter must be thoroughly measured to ensure the predictive capabilities of the model. Moreover, the composition of exhaust gases from the pilot flame have a significant influence on the pyrolysate ignition. As this composition is directly related to the burner operation parameters, these results suggest that the calibration method has an impact on the composite thermal degradation.

It is worth noting that the comparison of predicted and experimental time-to-ignition and backface temperature is not sufficient to fully validate the approach developed here, considering the important number of input parameters and processes involved. Nevertheless, this test-case demonstrates the proof-of-concept of the ability of the numerical tool to predict theoretically crucial parameters such as time-to-ignition and heat feedback from pyrolysate combustion, while limiting the use of empirical methods. In a future work, the authors intend to apply this numerical approach to model several fire tests, involving different materials and pilot flames to demonstrate the capacity of the architecture to be adaptable to different conditions and therefore validate the approach.

Desirable improvements to the model could include a better quantitative measurement of pyrolysate composition, including time dependence of each gaseous species as a function of the matrix temperature and degradation degree. A two-dimensional modeling could also allow to investigate pyrolysate ignition at some radial distance from the stagnation point, in locations with higher pyrolysate concentration and lower strain rate. Moreover, the same coupled architecture could be applied on the cold face of the material to predict the backface ignition, which is an important failure criterion in aerospace materials certification [3].

Acknowledgments

We are grateful for the assistance and financial support from the Natural Sciences and Engineering Research Council of Canada (NSERC/CRSNG), through grant no. CRDPJ 478687-15, from the Government Department for Formation and Research (Germany), through grant Jülich (PTJ) 03INT504BB and the partners from CRIAQ ENV-708 project is acknowledged. One of the authors (PCG) is grateful to the National Science and Technology Council of Mexico (CONACYT) for his doctoral scholarship.

References

[1] L. Nicolais, M. Meo, and E. Milella, *Composite materials: A Vision for the Future.* springer ed., 2011.

[2] K. V. Pochiraju, G. Tandon, and G. A. Shoeppner, *Long-Term Durability of Polymeric Matrix Composites.* 2012.

[3] ISO2685:1998(E), "Aircraft - Environmental Test Procedure for Airborne Equipment - Resistance to Fire in Designated Fire Zones," *the International Organization for Standardization (ISO): Geneva, Switzerland*, 1998.

[4] A. Mouritz, S. Feih, E. Kandare, Z. Mathys, A. Gibson, P. Des Jardin, S. Case, and B. Y. Lattimer, "Review of fire structural modelling of polymer composites," *Composites Part A: Applied Science and Manufacturing*, vol. 40, no. 12, pp. 1800–1814, 2009.

[5] A. L. Brown, "The Decomposition Behavior of Thermoset Carbon Fiber Epoxy Composites in the Fire Environment," in *Combustion Institute Joint US Sections Meeting May 19-22*, pp. 1–18, 2013.

[6] A. Mouritz and A. Gibson, *Fire Properties of polymer composite materials.* springer ed., 2006.

[7] K. Mcgrattan, S. Hostikka, R. Mcdermott, J. Floyd, C. Weinschenk, and K. Overholt, "Fire Dynamics Simulator User's Guide," 2016.

[8] C. Lautenberger and A. Fernandez-Pello, "Generalized pyrolysis model for combustible solids," *Fire Safety Journal*, vol. 44, no. 6, pp. 819–839, 2009.

[9] A. Snegirev, V. Talalov, V. Stepanov, and J. Harris, "A new model to predict pyrolysis, ignition and burning of flammable materials in fire tests," *Fire Safety Journal*, vol. 59, pp. 132–150, 2013.

[10] S. I. Stoliarov, I. T. Leventon, and R. E. Lyon, "Two-dimensional model of burning for pyrolyzable solids," *Fire and Materials*, 2014.

[11] R. D. Chippendale, I. O. Golosnoy, and P. L. Lewin, "Numerical modelling of thermal decomposition processes and associated damage in carbon fibre composites," *Journal of Physics D: Applied Physics*, vol. 47, no. 38, 2014.

[12] V. Biasi, *Modelisation Thermique de la Dégradation d'un Matériau Composite Soumis au Feu.* Thèse de doctorat, Université de Toulouse, 2014.

[13] M. Mckinnon, Y. Ding, S. I. Stoliarov, S. Crowley, and R. E. Lyon, "Pyrolysis model for a carbon fiber/epoxy structural aerospace composite," *Journal of Fire Sciences*, vol. 1, 2016.

[14] N. Grange, P. Tadini, K. Chetehouna, N. Gascoin, I. Reynaud, and S. Senave, "Determination of thermophysical properties for carbon-reinforced polymer-based composites up to 1000C," *Thermochimica Acta*, vol. 659, no. October 2017, pp. 157–165, 2018.

[15] A. Gibson, T. Browne, S. Feih, and A. Mouritz, "Modeling composite high temperature behavior and fire response under load," *Journal of Composite Materials*, vol. 46, no. 16, pp. 2005–2022, 2012.

[16] D. Sikoutris, D. Vlachos, V. Kostopoulos, S. Jagger, and S. Ledin, "Fire burnthrough response of CFRP aerostructures. Numerical investigation and experimental verification," *Applied Composite Materials*, vol. 19, no. 2, pp. 141–159, 2012.

[17] P. Tranchard, F. Samyn, S. Duquesne, B. Estèbe, and S. Bourbigot, "Modelling behaviour of a carbon epoxy composite exposed to fire: Part ii-comparison with experimental results," *Materials*, vol. 10, no. 5, 2017.

[18] W. Xie and P. DesJardin, "An embedded upward flame spread model using 2D direct numerical simulations," *Combustion and Flame*, vol. 156, pp. 522–530, 2009.

[19] C. Luo, W. Xie, and P. DesJardin, "Fluid-Structure Simulations of Composite Material Response for Fire Environments," *Fire Technology*, vol. 47, no. 4, pp. 887–912, 2011.

[20] G. Boyer, "Fully coupled CFD simulation of the pyrolysis of non-charring polymers: A predictive approach," *Fire Safety Journal*, pp. 1–10, 2017.

[21] T. Pelzmann, M. Kelly, S. Hind, M. Lévesque, and E. Robert, "The BTU Heat Transfer Device: Adapting a Standard Tool in Aircraft Fire Testing to Small Scale Experiments," *Ninth Triennial International Fire & Cabin Safety Research Conference of FAA*, 2019.

[22] C. Lautenberger, Y. Zhou, and A. Fernandez-Pello, "Numerical Modeling of Convective Effects on Piloted Ignition of Composite Materials," *Combustion Science and Technology*, vol. 177, no. 5-6, pp. 1231–1252, 2006.

[23] D. M. Marquis, E. Guillaume, A. Camillo, T. Rogaume, and F. Richard, "Existence and uniqueness of solutions of a differential equation system modeling the thermal decomposition of polymer materials," *Combustion and Flame*, vol. 160, no. 4, pp. 818–829, 2013.

[24] N. Tian and A. Zhou, "An ignition criterion for combustible solids integrating surface temperature and heating rate," *Fire and materials*, no. August 2008, p. 4B, 2014.

[25] M. McGurn, P. E. Desjardin, and A. B. Dodd, "Numerical simulation of expansion and charring of carbon-epoxy laminates in fire environments," *International Journal of Heat and Mass Transfer*, vol. 55, no. 1-3, pp. 272–281, 2012.

[26] J. G. Quintiere, "A simulation model for fire growth on materials subject to a room-corner test," *Fire Safety Journal*, vol. 20, no. 4, pp. 313–339, 1993.

[27] G. P. Smith, D. M. Golden, M. Frenklach, N. W. Moriarty, B. Eiteneer, M. C. Goldenberg, T. Bowman, R. K. Hanson, S. Song, W. C. Gardiner, V. V. Lissianski, and Z. Qin, "GRI-Mech," *http://www.me.berkeley.edu/gri_mech/*.

[28] Z. Mei, J. Mi, F. Wang, and C. Zheng, "Dimensions of CH4-jet flame in hot O2/CO2 coflow," *Energy and Fuels*, vol. 26, no. 6, pp. 3257–3266, 2012.

[29] W. P. Law and J. Gimbun, "Thermal performance enhancement of non-premixed syngas combustion in a partial combustion unit by winged nozzle: Experimental and CFD study," *Energy*, vol. 182, pp. 148–158, 2019.

[30] D. Goodwin, H. Moffat, and R. Speth, "Cantera: An Object-oriented Software Toolkit for Chemical Kinetics, Thermodynamics, and Transport Processes," *http://www.cantera.org, 2017. Version 2.3.0.*, 2017.

[31] W. Li, H. Huang, and X. Xu, "A coupled thermal/fluid/chemical/ablation method on surface ablation of charring composites," *International Journal of Heat and Mass Transfer*, vol. 109, pp. 725–736, 2017.

[32] J. Quintiere and M. Harkleroad, "New Concepts for Measuring Flame Spread Properties," *Fire Safety: Science and Engineering*, pp. 239–267, 1985.

[33] Y. Chen, M. Motevalli, and M. A. Delichatsios, "Material Pyrolysis Properties, Part I: An Integral Model for One-Dimensional Transient Pyrolysis of Charring and Non-Charring Materials," *Combustion Science and Technology*, vol. 88, no. 5-6, pp. 309–328, 1993.

[34] E. Kim and N. Dembsey, "Engineering Guide for Estimating Material Pyrolysis Properties for Fire Modeling," *Project final Report*, no. September, p. 382, 2012.

[35] K. S. Chen and R. Z. Yeh, "Pyrolysis kinetics of epoxy resin in a nitrogen atmosphere," *Journal of Hazardous Materials*, vol. 49, no. 2-3, pp. 105–113, 1996.

[36] P. Tranchard, F. Samyn, S. Duquesne, B. Estèbe, and S. Bourbigot, "Modelling behaviour of a carbon epoxy composite exposed to fire: Part I-Characterisation of thermophysical properties," *Materials*, vol. 10, no. 5, 2017.

[37] V. K. Sin and T. Y. Tong, "Comparison of numerical simulation of 2-D stagnation-point flow with similarity solution," *AIP Conference Proceedings*, vol. 1048, no. 2008, pp. 763–766, 2008.

[38] W. R. Smith and R. W. Missen, *Chemical Reaction Equilibrium Analysis: Theory and Algorithms*. Krieger Pub Co, reprint ed., 1991.

[39] J. Maxwell, *A treatise on Electricity and Magnetism*. 1954.

[40] W. Clayton, "Constituent and composite thermal conductivities of phenolic-carbon and phenolic-graphite ablators," *AIAA Paper 71-380*, 1971.

[41] A. Dasgupta, R. K. Agarwal, and S. M. Bhandarkar, "Three-dimensional modeling of woven-fabric composites for effective thermo-mechanical and thermal properties," *Composites Science and Technology*, vol. 56, no. 3, pp. 209–223, 1996.

[42] X. Maldague and S. Marinetti, "Pulse phase infrared thermography," *Journal of Applied Physics*, vol. 79, no. 5, pp. 2694–2698, 1996.

[43] M. Chaos, "Application of sensitivity analyses to condensed-phase pyrolysis modeling," *Fire Safety Journal*, vol. 61, pp. 254–264, 2013.

[44] H. K. Chelliah, A. Makino, I. Kato, N. Araki, and C. K. Law, "Modeling of graphite oxidation in a stagnation-point flow field using detailed homogeneous and semiglobal heterogeneous mechanisms with comparisons to experiments," *Combustion and Flame*, vol. 104, no. 4, pp. 469–480, 1996.

[45] N. Grange, K. Chetehouna, N. Gascoin, A. Coppalle, I. Reynaud, and S. Senave, "One-dimensional pyrolysis of carbon based composite materials using FireFOAM," *Fire Safety Journal*, vol. 97, no. April 2017, pp. 66–75, 2018.

[46] S. Vyazovkin, K. Chrissafis, M. L. Di Lorenzo, N. Koga, M. Pijolat, B. Roduit, N. Sbirrazzuoli, and J. J. Suñol, "ICTAC Kinetics Committee recommendations for collecting experimental thermal analysis data for kinetic computations," *Thermochimica Acta*, vol. 590, pp. 1–23, 2014.

[47] G. Jiang, S. J. Pickering, G. S. Walker, N. Bowering, K. H. Wong, and C. D. Rudd, "Soft ionisation analysis of evolved gas for oxidative decomposition of an epoxy resin/carbon fibre composite," *Thermochimica Acta*, vol. 454, no. 2, pp. 109–115, 2007.

[48] T. Ahamad and S. M. Alshehri, "Thermal degradation and evolved gas analysis of epoxy (DGEBA)/ novolac resin blends (ENB) during pyrolysis and combustion," *Journal of Thermal Analysis and Calorimetry*, vol. 111, pp. 445–451, 2013.

[49] B. Schartel, A. I. Balabanovich, U. Braun, U. Knoll, J. Artner, M. Ciesielski, M. Döring, R. Perez, J. K. W. Sandler, V. Altstädt, T. Hoffmann, and D. Pospiech, "Pyrolysis of Epoxy Resins and Fire Behavior of Epoxy Resin Composites Flame-Retarded with 9,10-Dihydro-9- oxa-10-phosphaphenanthrene-10-oxide Additives," *Journal of Applied Polymer Science*, vol. 104, no. 7, pp. 2260–2269, 2007.

[50] T. Fateh, J. Zhang, M. Delichatsios, and T. Rogaume, "Experimental investigation and numerical modelling of the fire performance for epoxy resin carbon fibre composites of variable thicknesses," *Fire and Materials*, no. June 2016, pp. 307–322, 2016.

[51] E. Robert, "Mass spectrometer calibration over wide concentration ranges in multicomponent gas mixtures," *Measurement Science and Technology*, vol. 21, no. 2, p. 025102, 2009.

[52] FAA, "Powerplant Installation and Propulsion System Component Fire Protection Test Methods, Standards, and Criteria," tech. rep., 2005.

[53] J. B. Henderson, J. A. Wiebelt, and M. R. Tant, "A Model for the Thermal Response of Polymer Composite Materials with Experimental Verification," *Journal of Composite Materials*, vol. 19, no. 6, pp. 579–595, 1985.

[54] S. Hu, J. Gao, Y. Zhou, C. Gong, X. S. Bai, Z. Li, and M. Alden, "Numerical and Experimental Study on Laminar Methane/Air Premixed Flames at Varying Pressure," *Energy Procedia*, vol. 105, pp. 4970–4975, 2017.

[55] É. Robert, *Experimental Investigation of Unstrained Diffusion Flames and their Instabilities.* PhD thesis, École Polytechnique Fédérale de Lausanne, 2008.

[56] J. M. Bergthorson, *Experiments and Modeling of Impinging Jets and Premixed (Ph.D. Thesis).* PhD thesis, California Institute of Technology, 2005.

[57] T. Fiala and T. Sattelmayer, "Non-Premixed Counterflow Flame Simulations: Scaling Rules for Fast Batch Simulations," *Hindawi Publishing Corporation Journal of Combustion*, vol. 2014, pp. 1–7, 2014.

[58] J. Bear, S. Kakaç, B. Kilkis, and F. A. Kulacki, "Modelling transport phenomena in porous media," in *Convective Heat and Mass Transfer in Porous Media*, ch. 1, pp. 7–71, 1991.

[59] M. A. Zanoni, J. L. Torero, and J. I. Gerhard, "The role of local thermal non-equilibrium in modelling smouldering combustion of organic liquids," *Proceedings of the Combustion Institute*, vol. 000, pp. 1–9, 2018.

[60] M. Looyeh, P. Bettess, and A. Gibson, "A one-dimensional finite element simulation for the fire-performance of GRP panels for offshore structures," *International Journal of Numerical Methods for Heat & Fluid Flow*, vol. 7, pp. 609–625, 1997.

[61] C. Baukal and B. Gebhart, "A review of semi-analytical solutions for flame impingement heat transfer," *International Journal of Heat and Mass Transfer*, vol. 39, no. 14, pp. 2989–3002, 1995.

[62] H. Martin, "Heat and Mass Transfer between Impinging Gas Jets and Solid Surfaces," *Advances in Heat Transfer*, 1977.

[63] P. S. Shadlesky, "Stagnation Point Heat Transfer for Jet Impingement to a Plane Surface," *AIAA Journal*, vol. 21, no. 8, pp. 1214–1215, 1982.

[64] D. A. Nield, *Convection in Porous Media.* 4th ed., 2013.

[65] J. A. Hubbard, A. L. Brown, A. B. Dodd, S. Gomez-vasquez, and C. J. Ramirez, "Carbon fiber composite characterization in adverse thermal environments," tech. rep., Sandia National Laboratory, 2011.

[66] J. R. Welty, C. E. Wicks, R. E. Wilson, and G. L. Rorrer, *Fundamentals of Momentum, Heat, and Mass Transfer.* 2008.

[67] J. Reddy and D. Gartling, *The Finite Element Method in Heat Transfer and Fluid Dynamics, 3rd edition.* CRC Press, taylor & f ed., 2010.

[68] M. Looyeh and P. Bettess, "A finite element model for the fire-performance of GRP panels including variable thermal properties," *Finite Elements in Analysis and Design*, vol. 30, no. 4, pp. 313–324, 1998.

[69] M. Looyeh, *Finite element simulation of heat flow in decomposing polymer composites.* Phd thesis, Durham University, 1999.

[70] M. Looyeh, K. Rados, and P. Bettess, "Thermochemical responses of sandwich panels to fire," *Finite Elements in Analysis and Design*, vol. 37, no. 11, pp. 913–927, 2001.

[71] P. Krysl, W. T. Ramroth, L. K. Stewart, and R. J. Asaro, "Finite element modelling of fibre reinforced polymer sandwich panels exposed to heat," *International Journal for Numerical Methods in Engineering*, vol. 61, no. 1, pp. 49–68, 2004.

[72] Y. Ng, J. Tomblin, and E. Lian, "Medium Temperature, Out-of-Autoclave, Oven-Vacuum-Bag Cure Epoxy Resin Impregnated Fiber Reinforced Composite Materials, Type 36, Class 2, Grade 193, Style 3k-70-PW," tech. rep., National Center for Advanced Materials Performance - NIAR Wichita State University, 2017.

[73] A. Kollmannsberger, R. Lichtinger, F. Hohenester, C. Ebel, and K. Drechsler, "Numerical analysis of the temperature profile during the laser-assisted automated fiber placement of CFRP tapes with thermoplastic matrix," *Journal of Thermoplastic Composite Materials*, vol. 31, no. 12, pp. 1563–1586, 2018.

[74] S. Hind, *Predicting and Measuring Thermal Conductivity in Carbon/Epoxy Unidirectional Tape and Textile Reinforced Composites.* PhD thesis, 2010.

[75] S. Vyazovkin, A. K. Burnham, J. M. Criado, L. A. Pérez-Maqueda, C. Popescu, and N. Sbirrazzuoli, "ICTAC Kinetics Committee recommendations for performing kinetic computations on thermal analysis data," *Thermochimica Acta*, vol. 520, no. 1-2, pp. 1–19, 2011.

[76] J. Langot, P. Chavez-Gomez, M. Levesque, and E. Robert, "Modeling the thermal degradation and residual mass of a carbon fiber epoxy matrix composite with a phenomenological approach: effect of the reaction scheme," *Submitted to Fire and Materials*, pp. 1–21, 2020.

[77] J. A. Quintiere, R. N. Walters, and S. Crowley, "Flammability Properties of Aircraft Carbon-Fiber Structural Composite," Tech. Rep. October, Federal Aviation Administration, 2007.

[78] M. Matalon, "On Flame Stretch," *Combustion Science and Technology*, vol. 31, pp. 169–181, 1983.

[79] R. Acharya and K. K. Kuo, "Effect of pressure and propellant composition on graphite rocket nozzle erosion rate," *Journal of Propulsion and Power*, vol. 23, no. 6, pp. 1242–1254, 2007.